Distinct magnetic fabric in weakly deformed sediments from extensional basins and fold-and-thrust structures in the Northern Apennine orogenic belt (Italy)

Chiara Caricchi, Francesca Cifelli, Catherine Kissel, Leonardo Sagnotti, Massimo Mattei

AGU PUBLICATIONS

Tectonics

RESEARCH ARTICLE
10.1002/2015TC003940

Key Points:
- We compare magnetic fabric from diversified deposits in the same orogenic system
- Measured AMS from Northern Apennines is typical of weakly deformed sediments
- A close relationship between magnetic fabric and tectonics is observed

Correspondence to:
C. Caricchi,
chiara.caricchi@ingv.it

Citation:
Caricchi, C., F. Cifelli, C. Kissel, L. Sagnotti, and M. Mattei (2016), Distinct magnetic fabric in weakly deformed sediments from extensional basins and fold-and-thrust structures in the Northern Apennine orogenic belt (Italy), *Tectonics*, *35*, 238–256, doi:10.1002/2015TC003940.

Received 8 JUN 2015
Accepted 8 JAN 2016
Accepted article online 12 JAN 2016
Published online 6 FEB 2016

Distinct magnetic fabric in weakly deformed sediments from extensional basins and fold-and-thrust structures in the Northern Apennine orogenic belt (Italy)

Chiara Caricchi[1,2], Francesca Cifelli[1], Catherine Kissel[3], Leonardo Sagnotti[2], and Massimo Mattei[1]

[1]Dipartimento di Scienze, Università Roma Tre, Rome, Italy, [2]Now at Istituto Nazionale di Geofisica e Vulcanologia, Rome, Italy, [3]Laboratoire des Sciences du Climat et de l'Environnement/IPSL, CEA-CNRS-UVSQ, Université Paris-Saclay, Gif-sur-Yvette, France

Abstract We report on results from anisotropy of magnetic susceptibility (AMS) analyses carried out on weakly deformed fine-grained sediments from the Northern Apennine orogenic system (Italy). We sampled 63 sites from preorogenic, synorogenic, and postorogenic sequences, which differ in age, composition, depositional environment, degrees of deformation, and tectonic regimes. The magnetic fabric is typical of weakly deformed sediments, with a magnetic foliation subparallel to the bedding plane and a magnetic lineation well defined in this plane. Northern Apennine chain deposits are characterized by strongly oblate magnetic susceptibility ellipsoids, indicating that the magnetic fabric is the result of both compaction process and tectonic load experienced by the sediments during diagenesis and orogenic events. The orientation of magnetic lineation is significantly different depending whether the studied sites underwent extensional or compressional tectonic regimes. In the Northern Apennine chain, the magnetic lineation is mostly oriented NNW-SSE, parallel to the main compressional structures. It suggests a tectonic origin of the magnetic lineation with an acquisition related to the Apennines compressional phases. In the extensional Tuscan Tyrrhenian margin, magnetic lineation is oriented ENE-WSW, almost perpendicular to the main extensional faults, which represent the main deformation elements of the area. Our results demonstrate a close relationship between the shape and orientation of magnetic fabric and the tectonic history of rocks, confirming that AMS represents a valuable tool to investigate the tectonic history of weakly deformed sedimentary rocks.

1. Introduction

Since *Graham* [1966] suggested the possibility to use the anisotropy of magnetic susceptibility (AMS) to reconstruct the deformation history of rocks, a large number of studies have been published concerning the relationships between magnetic fabric and tectonics [*Kissel et al*., 1986; *Rochette et al*., 1992; *Borradaile and Henry*, 1997; *Parés et al*., 1999; *Tarling and Hrouda*, 1993, among many others]. It has been largely demonstrated that in completely undeformed sediments, the magnetic susceptibility ellipsoid is oblate, with the magnetic foliation parallel to the bedding, as a consequence of depositional and/or compaction processes (see *Parés* [2015] for a recent review). In these conditions the presence of a magnetic lineation and the imbrication of magnetic foliation can be related to sedimentary processes, indicating the bottom current direction during deposition [e.g., *Rees*, 1965; *Schieber and Ellwood*, 1988; *Kissel et al*., 1997, 2010]. If sediments undergo tectonic deformation, a tectonic subfabric will progressively develop, modifying the primary sedimentary magnetic fabric depending on the amount and the type of deformation. In particular, the magnetic fabric acquires a geometry and orientation, which is very often distinctive between extensional and compressional tectonic settings [*Mattei et al*., 1997].

In fold-and-thrust belts the evolution of the magnetic fabric is generally related to different degrees of layer parallel shortening (LPS), indicating that the modification of the original sedimentary fabric occurred during the early stages of deformation [e.g., *Weil and Yonkee*, 2009]. In this case, the shape and orientation of the magnetic fabric depend on the degree of shortening and the presence of tectonic foliation (cleavage). When the LPS deformation is low to moderate, the principal maximum axis K_{max} (magnetic lineation) tracks the intersection between LPS and bedding plane and aligns perpendicular to the shortening direction and subparallel to the regional structural trend [*Kissel et al*., 1986; *Borradaile*, 1988; *Aubourg et al*., 1991; *Rochette et al*., 1992; *Housen et al*., 1993; *Sagnotti et al*., 1998; *Cifelli et al*., 2009; *Oliva-Urcia et al*., 2009; *Larrasoaña et al*., 2011; *Tang et al*., 2012]. With increasing LPS the original sedimentary fabric is completely

overprinted and the magnetic fabric becomes purely tectonic: the magnetic foliation rotates away from the bedding plane and tends to orient parallel to the cleavage planes, whereas the magnetic lineation aligns along the stretching direction [*Kligfield et al.*, 1981; *Lowrie and Hirt*, 1987; *Housen and Van der Pluijm*, 1991; *Averbuch et al.*, 1992; *Hirt et al.*, 1995, 2000; *Lunemburg et al.*, 1999; *Debacker et al.*, 2004, 2009; *Tavani and Cifelli*, 2010; *Cifelli et al.*, 2013].

In extensional tectonic setting the main distinctive feature of magnetic fabric is represented by the development of a magnetic lineation that is generally oriented parallel to the stretching direction and orthogonal to the main system of basin-bounding normal faults [*Sagnotti et al.*, 1994; *Mattei et al.*, 1997, 2004; *Cifelli et al.*, 2004; *Balsamo et al.*, 2008; *Soto et al.*, 2007; *Oliva-Urcia et al.*, 2010a, 2010b]. In this case the magnetic fabric is related to the reorientation of the basal planes of the phyllosilicate grains due to the progressive extension and the magnetic lineation is an intersection lineation resulting from the girdling of the phyllosilicates basal planes that intersect with their common axis parallel to the stretching direction [*Cifelli et al.*, 2005, 2007].

Despite the very large amount of published papers focused on AMS in sedimentary rocks, a significant scientific debate still exists on the tectonic or sedimentary origin of the magnetic fabric observed in sedimentary rocks in which visible evidence of deformation is lacking. In these cases the interpretation of magnetic fabric is not trivial and the development of a magnetic lineation has been attributed to the activity of water currents flowing during deposition [*Hamilton and Rees*, 1970; *Rees and Woodall*, 1975; *Ellwood*, 1980; *Taira*, 1989; *Tarling and Hrouda*, 1993; *Baas et al.*, 2007; *Parés et al.*, 2007; *Veloso et al.*, 2007; *Dall'Olio et al.*, 2013; *Cai et al.*, 2014] or to the reorientation of mineral particles during the early stages of deformation [*Lee et al.*, 1990; *Borradaile and Henry*, 1997; *Sagnotti and Speranza*, 1993; *Sagnotti et al.*, 1998; *Parés*, 2004; *Parés et al.*, 1999; *Kanamatsu et al.*, 2001; *Larrasoaña et al.*, 2004; *Weaver et al.*, 2004; *Cifelli et al.*, 2009; *Porreca and Mattei*, 2012; *Alimohammadian et al.*, 2013; *Cifelli et al.*, 2015]. Most of the difficulty to unambiguously interpret the magnetic fabric observed in weakly deformed sediments stems from the fact that most of these sediments, initially deposited in structurally controlled foredeep basins, are later incorporated in orogenic belts, showing a substantial parallelism between paleoflow directions and the orientation of fold axes [*Sagnotti et al.*, 1998; *Parés and Van der Pluijm*, 2002; *Dall'Olio et al.*, 2013].

So far, very few studies could discriminate between depositional/sedimentary and tectonic origin of the magnetic fabric [*Kissel et al.*, 1986; *Cifelli et al.*, 2015]. These results were obtained only from compressional areas, and no comparison of different sedimentary units, diversified for age, composition, depositional environment, degree of deformation, or tectonic regime, in the same orogenic system had been yet conducted.

In this work we present new magnetic analyses carried out in fine-grained sediments that experienced variable degrees of deformation in different tectonic regimes, from the Northern Apennine compression to the extension along the Tuscan Tyrrhenian margin (Figure 1). Our results allow us to better determine the origin of magnetic fabric in weakly deformed sedimentary units and to delineate the relationship between the orientation of magnetic lineation in fine-grained sediments and the tectonic structures in various extensional and compressional tectonic settings within the same orogen.

2. Geological and Tectonic Setting

The Northern Apennines chain is a fold-and-thrust belt resulting from the convergence between African (Adria microplate) and European plates [*Channell et al.*, 1979; *Bally et al.*, 1986; *Dewey et al.*, 1989; *Barchi et al.*, 1998a]. The evolution of the Northern Apennines proceeded with an eastward migration of the orogenic wedge, marked by the onset of foredeep basins filled by siliciclastic deposits that are progressively younger toward the Adriatic foreland [*Barchi et al.*, 1998a]. The Northern Apennine is composed of a series of stacked structural units accreted onto the Adriatic foreland [*Baldacci et al.*, 1967; *Elter*, 1975; *Boccaletti et al.*, 1980; *Principi and Treves*, 1984; *Barchi et al.*, 1998a; *Costa et al.*, 1998; *Molli et al.*, 2002] (Figure 1). The innermost and uppermost tectonostratigraphic unit is represented by oceanic (Ligurian unit) and transitional (sub-Ligurian) domains [*Elter*, 1975; *Bortolotti et al.*, 2001; *Cerrina Feroni et al.*, 2002], consisting of Jurassic ophiolite sedimentary rocks and Jurassic-early Cretaceous flysch deposits (helminthoid flysch) [*Elter*, 1975; *Marroni et al.*, 2001; *Festa et al.*, 2010]. The units from the Ligurian domain thrust onto the Tuscan units, formed by Upper Triassic to Eocene marine carbonates and Oligocene-lower Miocene siliciclastic foredeep sequences. The latter are deformed in an array of thrust sheets that ultimately thrust over the Umbria-Marche-Romagna units. In the western sector of the Tuscan domain, extensional tectonic is

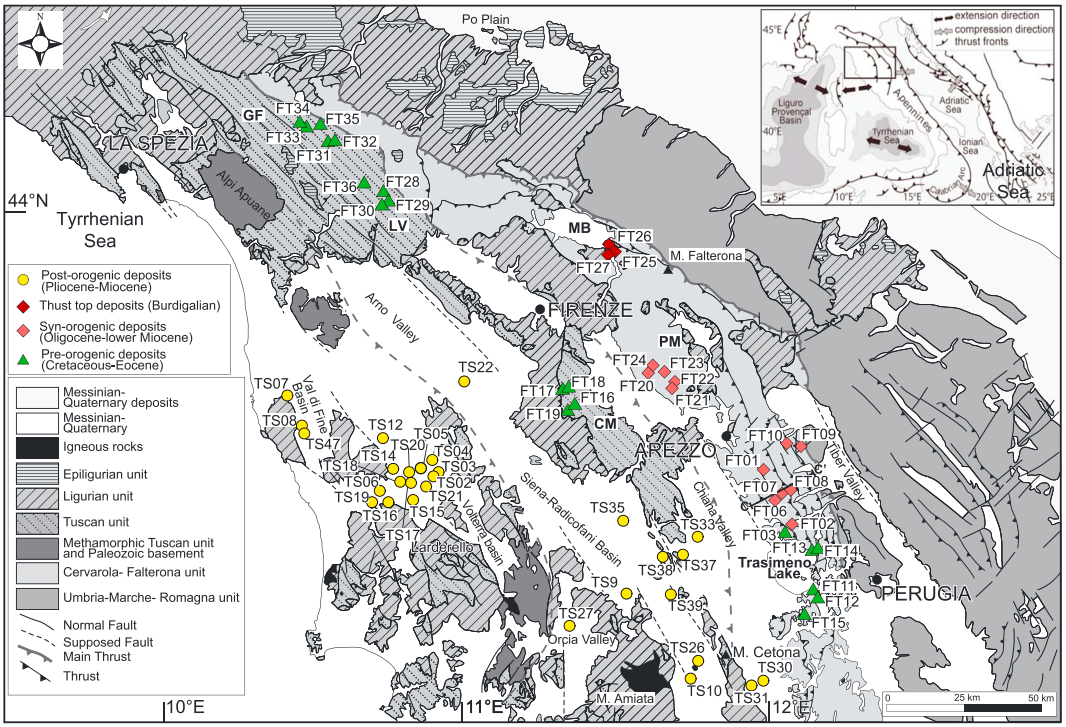

Figure 1. Schematic map of the Northern Apennines and location of the sampling sites.

coeval with the eastward thrust emplacement in the external Umbria-Marche-Romagna chain, [e.g., *Elter*, 1975] with both extensional and compressional fronts migrating toward the Adriatic foreland from middle Miocene until Pleistocene. This extensional tectonic phase is related to the opening of Tyrrhenian Sea back-arc basin [*Boccaletti et al*., 1980; *Malinverno and Ryan*, 1986; *Dewey et al*., 1989; *Barchi et al*., 1998b; *Faccenna et al*., 2004]. It dissected the already formed Apennine chain, generating new NW-SE trending extensional basins filled by "neo-autochthonous" marine and continental sequences [*Jolivet et al*., 1998; *Collettini et al*., 2006, and references therein]. Crustal thinning, high heat flow, and upraise of magmatic bodies accompanied extensional tectonics along the Tyrrhenian margin. NW-SE normal faults, mostly located in the internal sector of the Umbria-Marche-Romagna region, at the edges of the intramontane basins, represent the most important active tectonic features of the area with a well-documented historical and recent seismicity [e.g., *Chiaraluce et al*., 2004].

3. Sampling and Methods

Samples were drilled with an ASC 280E petrol-powered portable drill at 63 sites. The cores were distributed as widely as possible over the outcrops and oriented in situ with a magnetic compass. The magnetic orientations were corrected by about 2° to account for the local declination at the time of sampling.

Twenty-nine sites were sampled in postorogenic Messinian and Plio-Pleistocene blue clays, deposited in marine or lacustrine environments in the extensional basins along the Tuscan Tyrrhenian margin. In this area the neo-autochthonous sedimentary sequences are floored by upper Tortonian continental sequences, which transgressed onto the deformed units of the Apennine chain. These sequences are covered by lagoonal to marine sediments (conglomerates, sands, and clays) interbedded with Messinian evaporites. The upper part of the sequence consists of marine clastic deposits of Pliocene age. In the more internal part of the area some lacustrine basins developed in late Pliocene-Pleistocene, representing the younger sedimentary deposits of the Tuscan Tyrrhenian margin. In particular, we sampled eight sites in the upper Messinian blue clays from the Volterra, Val di Fine, and Orcia Valley basins and 21 sites in Pliocene blue clays mainly from Volterra and Siena-Radicofani basins (Figure 1).

In the internal sector of the Apennine chain 34 paleomagnetic sites were sampled from preorogenic, synorogenic, and thrust top deposits in the Tuscan succession, cropping out in the following areas: (i) around Lake Trasimeno, (ii) in Chianti Mountains (CM) and Pratomagno (PM) ridge, (iii) around the Mugello basin, and (iv) in Val di Lima (VL) and Garfagnana (GF) areas (Figure 1).

The preorogenic deposits consist of Upper Cretaceous-lower Eocene pelagic foreland ramp deposits characterized by calcareous marly turbidites and varicolored shales. Nineteen sites were sampled in varicolored shales and marly shale layers cropping out in Lake Trasimeno, Chianti Mountains, Garfagnana, and Val di Lima areas (Figure 1).

The synorogenic deposits consist of Rupelian-Aquitanian turbidites characterized by alternating thick coarse-grained and thin and fine-grained siliciclastic beds. In the Trasimeno Lake area and the Pratomagno ridge, 12 sites were collected from the thin and fine-grained beds (Figure 1).

Three sites were sampled in the Mugello Basin deposits (Figure 1), characterized by alternation between gray marls-silty marls and sandstone layers with calcareous component deposited in a Burdigalian thrust top basin.

AMS and rock magnetic analyses were carried out at the paleomagnetic laboratory of the Roma Tre University (Rome), Laboratoire des Sciences du Climat et de l'Environnement, (CEA/CNRS/UVSQ, Gif-sur-Yvette, France), and laboratory of paleomagnetism and rock magnetism of the Istituto Nazionale di Geofisica e Vulcanologia (INGV, Rome).

AMS is defined by a second rank tensor, and it is geometrically represented by a three-axis ellipsoid (with principal axes $K_{max} > K_{int} > K_{min}$), in which the long axis (K_{max}) represents the direction of largest induced magnetization and the short axis (K_{min}) the direction of lowest induced magnetization. Several parameters are used for the quantification of the magnitude of anisotropy and for defining the shape of the AMS ellipsoid (see Table 1) [*Jelinek*, 1981; *Hrouda*, 1982]. The mean susceptibility value K_m is computed as $K_m = (K_{max} + K_{int} + K_{min})/3$. T is the shape parameter and range from -1 (perfectly prolate ellipsoid with $L \gg F$) to +1 (perfectly oblate ellipsoid with $F \gg L$) with zero values corresponding to a triaxial shape ($F \sim L$, in which $K_{int}/K_{min} \sim K_{max}/K_{int}$). The anisotropy degree can be described by the parameter Pj [*Jelinek*, 1981], which considers all the three principal susceptibility values. Anisotropy of magnetic susceptibility (AMS) was measured for all samples using a KLY-3S Kappabridge magnetic susceptibility meter at the paleomagnetic laboratory at Roma TRE University and KLY-2 Kappabridge at Laboratoire des Sciences du Climat et de l'Environnement, (CEA/CNRS/UVSQ, Gif-sur-Yvette, France). Results are shown on an equal area stereographic projection using the *Jelínek and Kropáček* [1978] statistics. In order to identify the main magnetic minerals contributor to the AMS, we carried out a series of rock magnetic analyses on selected specimens. The measurements include (1) isothermal remanent magnetization (IRM) acquisition curves; (2) stepwise thermal demagnetization of a composite isothermal remanent magnetization (IRM) produced by sequential application of DC fields of 2.7 T, 0.6 T, and 0.12 T along three mutually orthogonal sample axes [*Lowrie*, 1990]; and (3) hysteresis properties of small rock fragments. Hysteresis properties were measured on a Micromag alternating gradient magnetometer (AGM model 2900, Princeton Measurements Corporation) with a maximum applied field of 1 T. For all the samples, the saturation magnetization (M_s), the saturation remanent magnetization (M_{rs}), and the coercive force (B_c) were determined after subtraction of the correction for the paramagnetic component contribution. The values of coercive remanent force (B_{cr}) were determined in a following experiment including a stepwise IRM acquisition at +1 T, followed by a stepwise application of a back field up to -1 T.

4. Results

4.1. Magnetic Properties

Different rock magnetic experiments were conducted in order to identify the ferromagnetic minerals in the sample, their grain size, and the paramagnetic contribution to the bulk susceptibility.

The stepwise acquisition of IRM (Figure 2a) indicates that IRM saturation is not reached by 900 mT for 19 samples of the preorogenic samples. This high-coercivity magnetic carrier is identified as hematite by the thermal demagnetization of three-axis IRM [*Lowrie*, 1990] which indicates a maximum unblocking temperature of ~680°C for the intermediate- and the high-coercivity fractions (Figure 2b). Six other preorogenic samples are characterized by an early IRM saturation (in fields around 0.3 T) and a maximum

AGU Tectonics

10.1002/2015TC003940

Table 1. List of Anisotropy Factors Computed at Each Site[a]

Site	Coordinates (Latitude-Longitude)	Lithology	Deposits	Age	N	S_0	K_m	L	F	P′	T	K_{max} (D, I)	K_{int} (D, I)	K_{min} (D, I)	E1−2	E2−3
							Trasimeno Lake Area									
FT01	43°20′48.3″, 12°02′09.2″	sand-limestone	synorogenic foredeep	Aquitanian	14	263,42	3.38E−04	1.009	1.095	1.117	0.822	305.1, 16.3	203.6, 34.5	56.2, 50.8	18.7	3.7
FT02	43°14′49.4″, 12°06′28.1″	sand-limestone	synorogenic foredeep	Aquitanian	11	246,30	3.05E−04	1.009	1.082	1.102	0.795	314.7, 5.3	221.6, 30.2	53.7, 59.2	6.3	2.5
FT03	43°14′32.3″, 12°04′54.9″	mudstone	preorogenic	Eocene	45	variable	3.61E−05	1.012	1.025	1.040	0.264	282.5, 16.4	186.0, 21.1	47.5, 62.8	60.3	14.0
FT06	43°17′53.5″, 12°02′22.6″	sand-limestone	synorogenic foredeep	Aquitanian	19	variable	2.27E−04	1.008	1.085	1.104	0.813	310.5, 2.4	218.5, 38.6	43.5, 51.3	34.2	4.9
FT07	43°17′57.2″, 12°02′30.4″	sand-limestone	synorogenic foredeep	Aquitanian	13	235,30	2.95E−04	1.007	1.087	1.106	0.851	147.9, 4.7	241.1, 34.1	51.1, 55.4	45.6	3.9
FT08	43°18′13.8″, 12°04′34.9″	mudstone	synorogenic foredeep	Aquitanian	12	variable	1.75E−04	1.010	1.076	1.095	0.773	160.5, 14.0	257.1, 24.8	43.7, 61.0	7.0	3.2
FT09	43°27′34.6″, 12°08′12.2″	mudstone	synorogenic foredeep	Aquitanian	14	230,21	1.43E−04	1.006	1.060	1.073	0.828	245.0, 25.8	146.4, 17.1	26.6, 58.3	22.2	2.6
FT10	43°27′46.8″, 12°07′40.3″	mudstone	synorogenic foredeep	Aquitanian	15	160,11	1.59E−04	1.005	1.067	1.080	0.869	101.4, 10.0	193.6, 12.4	333.5, 74.0	21.5	3.8
FT11	43°05′14.2″, 12°10′50.0″	mudstone	preorogenic	Eocene	13	variable	6.37E−06	0.841	0.883	1.079	0.071	355.0, 14.5	128.8, 69.5	261.3, 14.1	30.9	18.7
FT12	43°04′17.7″, 12°11′22.6″	mudstone	preorogenic	Eocene	16	variable	2.60E−05	1.018	1.028	1.049	0.182	345.5, 16.2	204.1, 69.7	79.1, 12.0	31.9	22.6
FT13	43°10′54.6″, 12°10′21.7″	mudstone	preorogenic	Eocene	17	variable	4.03E−05	1.014	1.052	1.072	0.531	350.2, 2.4	257.6, 47.4	82.4, 42.5	22.5	6.8
FT14	43°10′53.3″, 12°10′26.3″	mudstone	preorogenic	Eocene	11	variable	2.55E−05	1.021	1.037	1.061	0.275	165.0, 5.3	67.2, 55.9	258.5, 33.6	13.4	12.1
FT15	43°02′38.7″, 12°08′52.7″	mudstone	preorogenic	Eocene	68	variable	3.99E−05	1.006	1.023	1.032	0.477	304.4, 31.5	165.3, 50.9	47.8, 20.6	57.2	7.4
							Monti del Chianti e Pratomagno Area									
FT16	43°32′19.8″, 11°24′32.9″	mudstone	preorogenic	Eocene-Oligocene	13	248,09	7.29E−05	1.003	1.033	1.040	0.691	251,2/20,7	156,2/13.0	36.3/65.2	33.2	6.3
FT17	43°35′58.2″, 11°22′02.1″	mudstone	preorogenic	Eocene-Oligocene	11	73,17	5.42E−05	1.009	1.053	1.069	0.641	155.1/1.0	64.7/24.2	247.4/65.8	21.5	4.0
FT18	43°36′09.0″, 11°22′21.2″	mudstone	preorogenic	Eocene-Oligocene	13	24,23	4.26E−05	1.007	1.015	1.024	0.367	307.0/6.3	38.6/13.8	193.2/74.7	42.8	14.5
FT19	43°32′06.3″, 11°22′41.0″	mudstone	preorogenic	Eocene-Oligocene	11	220,22	6.77E−05	1.004	1.012	1.017	0.501	141.7/5.3	232.4/7.4	16.2/80.9	26.7	7.6
FT20	43°37′28.7″, 11°40′43.8″	sand-limestone	synorogenic foredeep	Chattian- Aquitanian	16	variable	2.60E−04	1.009	1.091	1.112	0.796	328.0/4.3	58.4/5.1	198.2/83.3	10.0	4.5
FT21	43°37′23.7″, 11°40′59.1″	sand-limestone	synorogenic foredeep	Chattian-Aquitanian	13	55,19	2.74E−04	1.012	1.066	1.085	0.665	333.0/8.2	65.5/17.1	218.3/71.0	16.3	5.7
FT22	43°37′40.2″, 11°41′00.1″	sand-limestone	synorogenic foredeep	Chattian-Aquitanian	11	variable	3.20E−04	1.010	1.106	1.131	0.824	127.9/3.6	37.2/11.2	235.5/78.2	33.0	4.0
FT23	43°38′13.5″, 11°40′30.8″	sand-limestone	synorogenic foredeep	Chattian-Aquitanian	9	70,11	1.62E−04	1.007	1.062	1.077	0.783	312.3/5.0	43.0/8.2	191.3/80.4	11.4	3.1
FT24	43°38′51.8″, 11°39′38.9″	sand-limestone	synorogenic foredeep	Chattian-Aquitanian	8	110,9	1.90E−04	1.008	1.075	1.093	0.797	143.3/4.3	53.0/4.4	277.2/83.8	10.7	0.9

AGU Tectonics

10.1002/2015TC003940

Table 1. (continued)

Site	Coordinates (Latitude-Longitude)	Lithology	Deposits	Age	N	S_0	K_m	L	F	P′	T	K_{max} (D, I)	K_{int} (D, I)	K_{min} (D, I)	E1−2	E2−3
							Mugello Basin Area									
FT25	43°55′43.1″, 11°29′57.9″	marls	thust top	Burdigalian-Langhian	12	340,25	8.81E−05	1.015	1.034	1.051	0.366	299.4/16.9	30.4/3.4	131.5/72.7	5.2	1.8
FT26	43°55′5.1″, 11°29′41.8″	marls	thust top	Burdigalian-Langhian	13	32,25	1.15E−04	1.017	1.031	1.049	0.286	297.2/1.9	28.4/32.2	204.2/57.7	7.8	3.7
FT27	43°54′48.8″, 11°27′14.8″	marls	thust top	Burdigalian-Langhian	12	80,10	1.31E−04	1.020	1.037	1.059	0.270	324.6/1.2	234.5/4.7	69.2/85.1	9.1	3.7
							Garfagnana Area									
FT28	44°01′53.1″, 10°43′04.1″	mudstone	preorogenic	middle Eocene	9	28,50[b]	4.46E−05	1.024	1.058	1.086	0.402	324.6/27.0	77.7/37.0	208.8/40.5	13.1	3.8
FT29	44°00′54.6″, 10°43′ 14.0″	mudstone	preorogenic	middle Eocene	9	250,26[b]	3.67E−05	1.013	1.071	1.093	0.681	316.1/7.7	222.7/24.1	62.6/64.5	25.0	4.2
FT30	44°01′14.9″, 10°43′07.2″	mudstone	preorogenic	Upper Cretaceous-Paleocene	9	283,22	2.49E−05	1.019	1.055	1.078	0.476	329.3/15	235.3/14.6	103/68.8	21.2	2.8
FT31	44°10′52.6″, 10°24′28.6″	mudstone	preorogenic	Upper Cretaceous-Paleocene	11	211,31[b]	2.60E−04	1.026	1.033	1.060	0.116	156.2/19	254.8/23.4	31.0/59.1	10.1	4.0
FT32	44°11′02.5″, 10°24′17.0″	mudstone	preorogenic	Upper Cretaceous-Paleocene	9	210.82[b]	1.50E−04	1.026	1.008	1.037	−0.439	122/9.3	260/77.6	30.7/8.2	15.4	2.7
FT33	44°11′02.5″, 10°24′17.0″	mudstone	preorogenic	Upper Cretaceous-Paleocene	9	263,37[b]	2.45E−04	1.016	1.055	1.075	0.534	178.4/3.6	271/36.7	83.5/53.1	8.0	2.6
FT34	44°12′50.5″, 10°22′19.6″	mudstone	preorogenic	Upper Cretaceous-Paleocene	10	283,36[b]	2.25E−04	1.008	1.056	1.071	0.751	354.4/13.2	255.7/32.6	103.4/54.1	6.8	4.1
FT35	44°12′44.9″, 10°24′43.1″	mudstone	preorogenic	Upper Cretaceous-Paleocene	12	39,29[b]	3.32E−04	1.015	1.091	1.117	0.714	318.2/4.6	50.7/28.5	219.8/61.1	17.5	5.1
FT36	44°04′27.8″, 10°35′28.5″	mudstone	preorogenic	middle Eocene	9	284,26[b]	1.38E−04	1.026	1.051	1.079	0.013	322.3/21.3	226.4/14.7	104.3/63.7	5.0	3.6
							Val di Fine Basin									
TS07	43°27′42.5″N, 10°24′42.6″E	blue clays	postorogenic	Messinian	6	6,25	1.15E−04	1.016	1.050	1.070	0.490	94.3, 11.8	359.1, 23.3	209.1, 63.5	40.6	6.3
TS08	43°26′16.7″N, 10°27′1.8″E	blue clays	postorogenic	Messinian	10	0,0	2.01E−04	1.003	1.028	1.035	0.707	224.3, 0.3	314.3, 4.6	11.9,8.2	60.3	8.2
TS47	43°26′00.9″N, 10°28′37.2″E	blue clays	postorogenic	Messinian	7		1.36E−04	1.005	1.020	1.027	0.604	82.8, 26.2	349.3, 7.2	245.2, 62.7	27.4	1.9
							Volterra Basin									
TS15	43°19′38.2″N, 10°44′16.2″E	blue clays	postorogenic	Messinian	8	207, 4	1.59E−04	1.017	1.030	1.049	0.165	247.9, 9.8	339.9, 11.4	118.0,74.9	14.0	7.7
TS16	43°18′50.0″N, 10°41′58.0″E	blue clays	postorogenic	Messinian	8	209, 27	1. 92E−04	1.005	1.057	1.070	0.800	255.3,19.3	161.7, 10.2	45.2, 68.0	14.8	2.1
TS17	43°19′55.6″N, 10°46′37.8″E	blue clays	postorogenic	Messinian	9	357, 9	2.11E−04	1.004	1.055	1.066	0.863	287.4, 5.6	197.2, 2.4	83.9, 83.9	41.3	1.5
TS18	43°20′45.1″N, 10°44′2.4″E	blue clays	postorogenic	Messinian	11	229, 49	2.19E−04	1.010	1.028	1.040	0.522	212.7, 59.2	310.5, 4.6	43.2, 30.4	28.4	2.3
TS21	43°19′47.2″N, 10°47′34.9″E	blue clays	postorogenic	Messinian	11	66, 19	1. 95E−04	1.006	1.021	1.028	0.557	24.8, 14.5	116.5, 6.4	229.7, 74.1	17.0	2.2
TS02	43°20′41.5″N, 10°48′50.7″E	blue clays	postorogenic	Pliocene	10	0, 20	1. 88E−04	1.005	1.031	1.039	0.726	31.8, 17.7	298.6, 10.0	180.4, 69.5	15.8	3.2
TS04	43°21′49.0″N, 10°45′22.9″E	blue clays	postorogenic	Pliocene	12	0,0	1. 88E−04	1.009	1.021	1.031	0.471	271.4, 3.2	1.7, 5.7	152.1, 83.5	17.5	4.6

AGU Tectonics

10.1002/2015TC003940

Table 1. (continued)

Site	Coordinates (Latitude-Longitude)	Lithology	Deposits	Age	N	S_0	K_m	L	F	P′	T	K_{max} (D, I)	K_{int} (D, I)	K_{min} (D, I)	E1−2	E2−3
TS05	43°21′11.9″N, 10°45′18.4″E	blue clays	postorogenic	Pliocene	10	XX	1. 68E−04	1.005	1.037	1.047	0.722	36.3, 7.0	305.9, 3.6	189.0, 82.1	73.2	5.3
TS06	43°20′32.8″N, 10°42′12.3″E	blue clays	postorogenic	Pliocene	11	272, 9	4.82E−04	1.019	1.043	1.064	0.392	302.7, 9.1	211.7, 6.1	88.4, 79.0	21.2	3.4
TS12	43°26′46.0″N, 10°43′35.5″E	blue clays	postorogenic	Pliocene	9	0,0	2.05E−04	1.005	1.032	1.041	0.717	6.4, 4.7	96.5, 1.2	200.5, 85.1	36.6	5.5
TS14	43°23′53.1″N, 10°45′3.7″E	blue clays	postorogenic	Pliocene	11	87.1, 1	1.58E−04	1.044	1.038	1.047	0.798	78.2, 10.0	168.4, 1.2	265.1, 79.9	55.3	4.3
TS19	43°19′19.4″N, 10°41′8.1″E	blue clays	postorogenic	Pliocene	12	280, 10	1.70E−04	1.006	1.021	1.028	0.540	4.2, 2.2	273.7, 11.1	105.1, 78.7	40.0	5.8
TS20	43°20′45.1″N, 10°44′2.4″E	blue clays	postorogenic	Pliocene	8	0,0	2.00E−04	1.014	1.034	1.051	0.447	65.4,6.1	155.7, 2.5	268.0, 83.4	19.0	11.0
TS03	42°12′12.0″N, 10°49′4.0″E	blue clays	postorogenic	Pliocene	9	0, 0	1.76E−04	1.008	1.036	1.047	0.619	59.5, 2.0	329.4, 4.2	174.4, 85.4	15.0	6.2
							Siena-Radicofani Basin									
TS22	42°44′57.0″N, 10°54′50.9″E	blue clays	postorogenic	Pliocene	14	-	1.88E−04	1.013	1.021	1.035	0.273	92.7, 3.9	2.2, 7.1	211.5, 81.9	11.9	3.2
TS10	42°50′58.0″N, 11°48′46.4″E	blue clays	postorogenic	Pliocene	9	XX	2.38E−04	1.015	1.023	1.039	0.203	39.4, 2.0	309.3, 0.6	201.5, 87.9	11.4	3.4
TS26	42°52′35.2″N, 11°49′44.6″E	blue clays	postorogenic	Pliocene	8	288, 8	2.39E−04	1.005	1.022	1.030	0.640	244.0, 1.5	334.2, 7.5	142.6, 82.4	28.2	8.6
TS31	42°51′36.2″N, 11°58′16.9″E	blue clays	postorogenic	Pliocene	9	0, 0	1.61E−04	1.009	1.018	1.028	0.413	48.2, 9.8	138.4, 1.4	236.4, 80.1	16.4	2.6
TS33	43°12′54.9″N, 11°47′43.4″E	blue clays	postorogenic	Pliocene	10	7, 6	2.85E−04	1.005	1.016	1.022	0.385	346.1, 5.7	76.4, 2.4	189.4, 83.8	24.1	4.7
TS35	43°12′25.1″N, 11°37′59.9″E	blue clays	postorogenic	Pliocene	8	0, 0	2.69E−04	1.011	1.024	1.037	0.439	81.1, 1.9	351.0, 3.2	202.0, 86.3	33.3	2.8
TS37	43°9′58.6″N, 11°46′6.0″E	blue clays	postorogenic	Pliocene	9	XX	1.69E−04	1.005	1.020	1.027	0.536	320.8, 3.2	51.0, 3.5	187.9, 85.3	17.3	5.6
TS38	43°10′27.5″N, 11°44′16.7″E	blue clays	postorogenic	Pliocene	9	XX	2.94E−04	1.010	1.023	1.034	0.421	127.2, 2.5	217.3, 2.0	346.4, 86.8	31.4	3.9
TS39	43°04′46.8″N, 11°42′23.2″E	blue clays	postorogenic	Pliocene	13	63, 16	1.98E−04	1.007	1.021	1.030	0.594	33.7, 14.0	125.1, 5.6	236.5, 74.9	36.1	4.8
TS09	43°03′51.7″N, 11°32′8.9″E	blue clays	postorogenic	Pliocene	5	214, 6	1.85E−04	1.003	1.022	1.028	0.790	56.4, 5.6	326.4, 0.5	231.6, 84.3	21.4	3.3
TS30	42°51′58.0″N, 11°58′46.1″E	blue clays	postorogenic	Pliocene	9	50, 8	1.44E−04	1.003	1.013	1.017	0.662	138.9, 2.5	48.6, 5.8	252.4, 83.7	38.3	4.7
							Orcia Valley									
TS27	42°56′36.9″N, 11°24′19.9″E	blue clays	postorogenic	Messinian	11	198,16	2.24E−04	1.006	1.019	1.027	0.483	248.7, 14.9	155.9, 10.3	32.4, 71.8	13.9	2.7

[a] N = number of specimens $k_m = (k_{max} + k_{int} + k_{min})/3$ (mean susceptibility, in 10^{-6} SI units); $L = k_{max}/k_{int}$; $F = k_{int}/k_{min}$. $P' = \exp\{2[(\eta_1 - \eta)^2 + (\eta_2 - \eta)^2 + (\eta_3 - \eta)^2]\}^{1/2}$ (corrected anisotropy degree) [*Jelinek*, 1981]. $T = 2(\eta_2 - \eta_3)/(\eta_1 - \eta_3) - 1$ (shape factor) [*Jelinek*, 1981]. $\eta_1 = \ln k_{max}$; $\eta_2 = \ln k_{int}$; $\eta_3 = \ln k_{min}$; $\eta = (\eta_1 + \eta_2 + \eta_3)/3$. D = declination, I = inclination. For each locality the line shows the site arithmetic mean values. S_0 bedding attitude (azimuth of the dip and dip values).

[b] Deduced by AMS tensor.

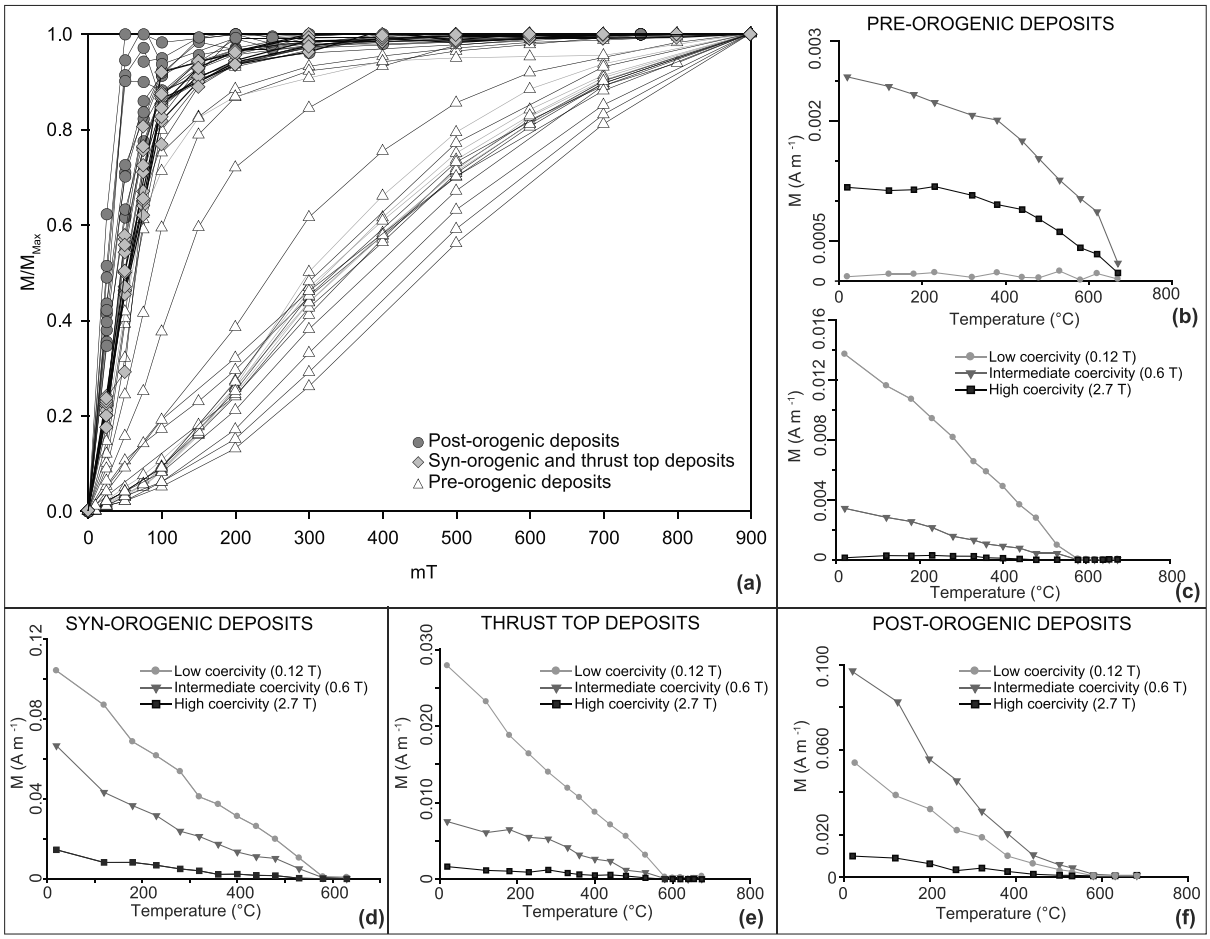

Figure 2. Main results from magnetic mineralogy analyses: (a) isothermal remanent magnetization (IRM) acquisition curves and (b–f) thermal demagnetization curves of a three-component (low-, intermediate-, and high-coercivity) IRM [*Lowrie*, 1990].

unblocking temperature around 580°C of the dominant IRM low-coercivity component (Figure 2c). This indicates that magnetite is the main remanence magnetic carrier in these samples. In synorogenic, thrust top, and postorogenic deposits, magnetite is also the main remanence carrier (Figures 2a, 2d, 2e, and 2f), but in a few postorogenic sites, the intermediate- and low-coercivity IRM components are unblocked between 320°C and 380°C, typical of ferromagnetic iron sulphides. The presence of greigite (Figure 2f) is confirmed by X-ray analysis performed on these samples.

Hysteresis analyses were carried out in order to evaluate the paramagnetic contribution to the low-field-induced magnetization and to obtain information about the domain state (i.e., average grain size of the magnetite/greigite) with the use of the Day diagram [*Day et al.*, 1977; *Dunlop*, 2002] (Figure 3). In the preorogenic samples characterized by hematite, hysteresis loops consistently show a distinct loop and high remanent coercivities (B_{cr} ~ 400 mT, Figure 3a). Hysteresis diagrams obtained for synorogenic and thrust top deposits are mainly linear showing a prevalent paramagnetic contribution (Figures 3b and 3c). The hysteresis loops obtained after correction for the paramagnetic slope are consequently poorly defined and indicate the presence of very low amounts of low-coercivity ferrimagnetic minerals. The obtained B_{cr} values (in the range 30–45 mT) (Figures 3b and 3c) and the available rock magnetic data [see also *Caricchi et al.*, 2014] indicate that the very weak remanent signal in these deposits is carried by magnetite. The hysteresis data of the postorogenic deposits indicate a distinct ferromagnetic (in a broad sense) contribution with the presence of low-coercivity minerals in the pseudosingle to multidomain range grain sizes (Figures 3d and 3e).

The mean magnetic susceptibility (K_m) values and anisotropy parameters of the analyzed sediments are listed in Table 1. K_m values range between 23×10^{-6} and 480×10^{-6} SI with most of the values below 200×10^{-6} SI.

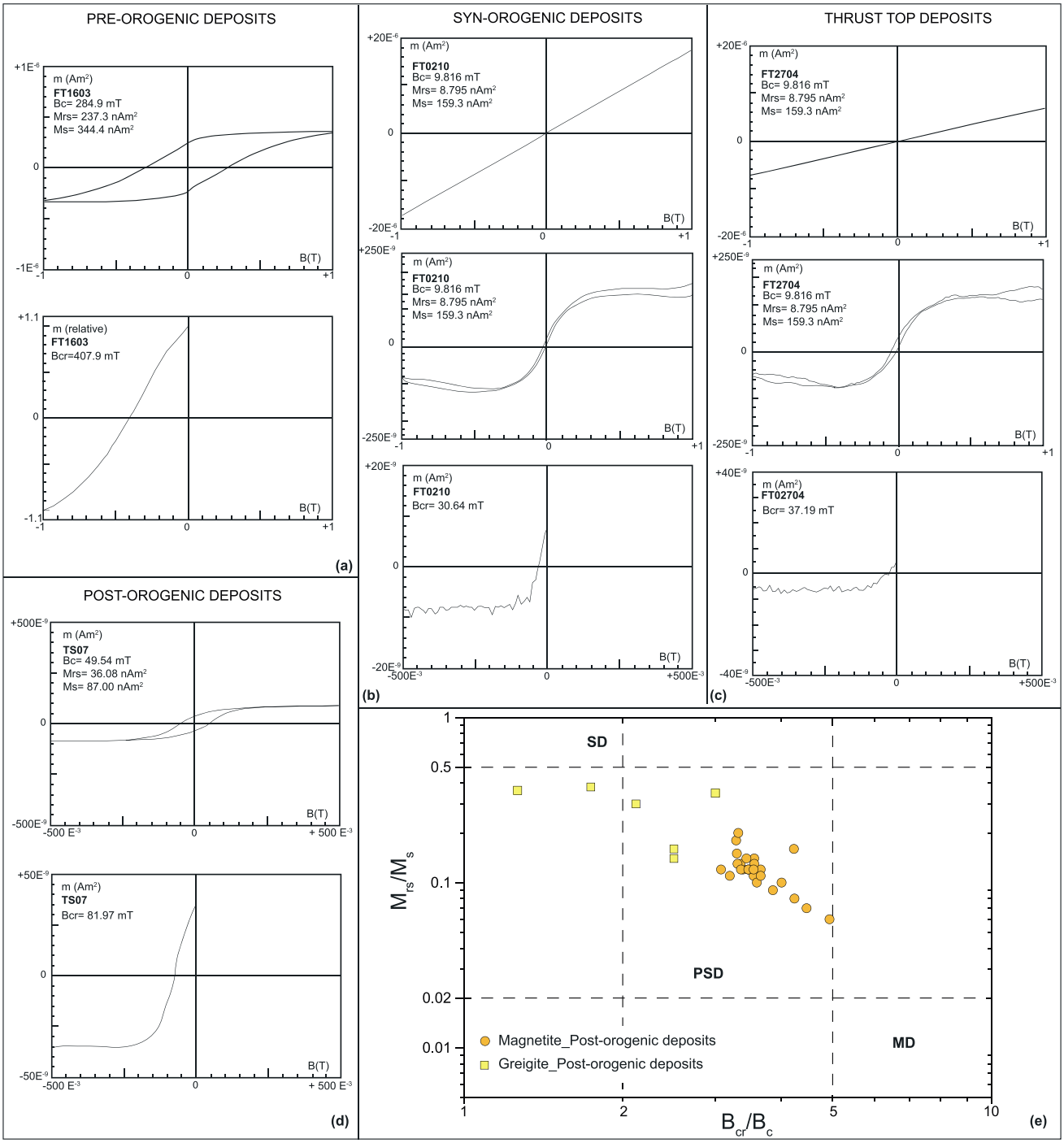

Figure 3. Hysteresis data for representative samples: (a) preorogenic deposits, (b) synorogenic deposits, (c) thrust top deposits, and (d) postorogenic deposits. Hysteresis loops for preorogenic and postorogenic deposits are well defined and are plotted after correction for the paramagnetic susceptibility (upper plots in Figures 3a and 3d). Samples from synorogenic and thrust top deposits are dominated by the paramagnetic fraction, and the hysteresis curves are quite linear (upper plots in Figures 3b and 3c). After subtraction of the paramagnetic slope and a 100X magnification, weak hysteresis loops are identifiable also for these samples (middle plots in Figures 3b and 3c). The lower plots in Figures 3a–3d show the back-field remagnetization curves up to −1 T, from which we estimated the coercivity of remanence (B_{cr}). (e) Plot of hysteresis ratios (M_{rs}/M_s versus B_{cr}/B_c; modified from *Dunlop* [2002]) for samples of postorogenic deposits. The indicated fields for single domain (SD), pseudosingle domain (PSD), and multidomain (MD) refer only to magnetite particles.

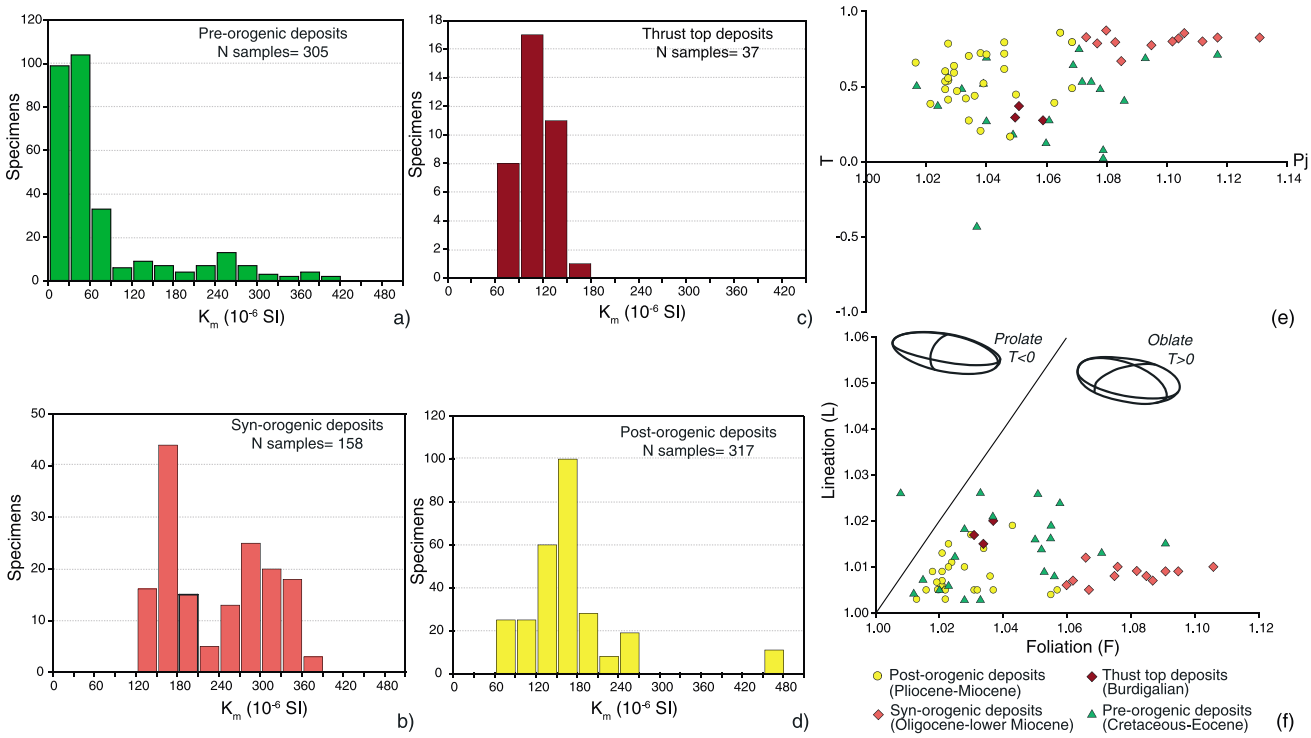

Figure 4. Frequency distribution of the mean susceptibility (K_m) values for (a) preorogenic deposits, (b) synorogenic deposits, (c) thrust top deposits, and (d) postorogenic deposits. (e) Plots of shape parameters (T) versus degree of anisotropy (Pj) and magnetic lineation (L) versus magnetic foliation (F) for all the investigated sites.

This range of variability indicates a prevailing contribution of the paramagnetic minerals of the rock matrix, with an overall low content of ferromagnetic (in a broad sense) minerals and in particular a negligible contribution of ferrimagnetic minerals [*Hrouda and Kahan*, 1991; *Tarling and Hrouda*, 1993]. This is confirmed by the comparison between low- and high-field susceptibility values, which do not differ by more than 20% (average 8%).

Figure 4 shows the distribution of the magnetic susceptibility values for all the analyzed deposits. Preorogenic deposits have the widest K_m distribution, with a main clustering at low values, between 0 and 90×10^{-6} SI, and a long tail up to 420×10^{-6} SI (Figure 4a). Most of the susceptibility values of the preorogenic samples are lower than those measured for the synorogenic ones. The latter show K_m values in the range between 100 and 400×10^{-6} SI and a bimodal distribution with two modes at $150–180 \times 10^{-6}$ SI and at $270–300 \times 10^{-6}$ SI (Figure 4b). The thrust top deposits display K_m values mainly clustered between 60 and 180×10^{-6} SI (Figure 4c), while the postorogenic Messinian-Pleistocene clay deposits are characterized by K_m values ranging between 60 and 290×10^{-6} SI with a single exception of one site (TS06) with K_m of $450–480 \times 10^{-6}$ SI (Figure 4d). Besides differences in the relative content and nature of ferromagnetic (in a broad sense) minerals, the observed different K_m distributions also reflect the different composition of the rock matrix. The low susceptibility values observed in the pelagic carbonates of the preorogenic deposits probably result from their large diamagnetic content (i.e., calcite). The paramagnetic contribution of the clay minerals prevails in the synorogenic deposits of foredeep basins, which show the highest susceptibility values, and in the blue clays of the postorogenic sediments deposited in extensional basins. The mean susceptibility values of the marly thrust top deposits reflect the contribution of both paramagnetic and diamagnetic minerals of the rock matrix. X-ray diffraction (XRD) quantitative analyses on whole-rock samples from previous studies [*Battaglia et al.*, 2002; *Meneghini et al.*, 2012; *Caricchi et al.*, 2015] indicate that all types of analyzed deposits are characterized by the presence of calcite, quartz, plagioclase, and phyllosilicates minerals in the rock matrix. Moreover, the XRD analyses of the <2 μm grain size fraction show a clay mineral assemblage constituted by illite, mixed layer illite-smectite, mixed layer illite-chlorite, kaolinite, and chlorite [*Battaglia et al.*, 2002; *Meneghini et al.*, 2012; *Caricchi et al.*, 2015].

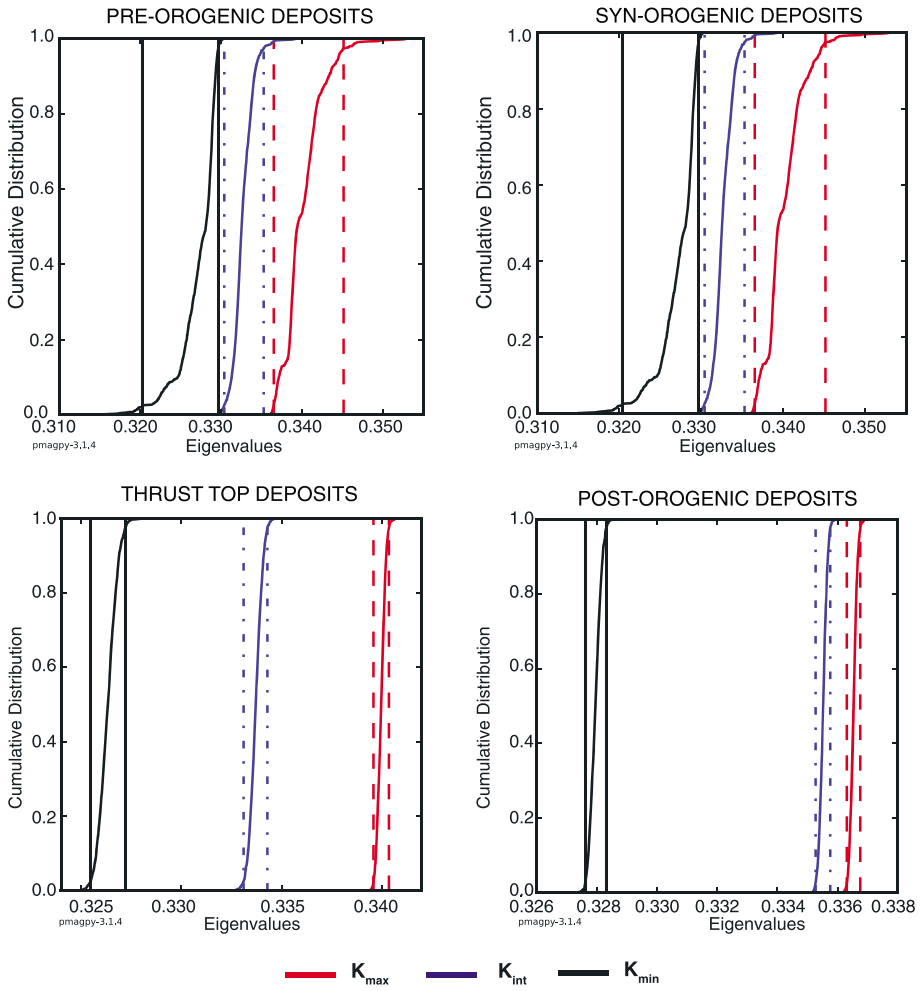

Figure 5. Results of bootstrap analyses. Cumulative distributions of K_{min}, K_{int}, and K_{max} (solid line) and their 95% confidence bounds (dash lines). In all cases the three eigenvalues and associate eigenvectors are distinct from one to another. In the case of postorogenic deposits $K_{min} \ll K_{int} < K_{max}$.

4.2. AMS Shape Parameters

The shape and eccentricity of the susceptibility ellipsoids have been evaluated by plotting *Pj* versus *T* (Figure 4e) and *L* versus *F* (Figure 4f). The preorogenic deposits show a large scattering of both shape (*T*) and anisotropy degree (*Pj*) parameters, with values varying from −0.439 to 0.751 and from 1.017 to 1.093, respectively (Table 1). Oblate AMS ellipsoids dominate in the preorogenic deposits, with only one exception (site FT32). In this case, the negative *T* value ($T = -0.439$) indicates a prolate fabric. A similar distribution for the *T* parameter (0.203–0.863) has been observed in the postorogenic deposits, indicating a prevalent oblate shape of the AMS ellipsoids, which, however, show a lower and less dispersed distribution of *Pj* values ($Pj = 1.017–1.070$). For thrust and synorogenic deposits, the *T* and *Pj* values are more clustered. The thrust top deposits have *T* values ranging from 0.270 to 0.366 and *Pj* values between 1.049 and 1.093, whereas the synorogenic sediments are characterized by *T* values comprised between 0.665 and 0.869, and *Pj* values between 1.073 and 1.117, recording the highest degree of magnetic anisotropy among the analyzed sequences. The distribution of both the foliation (*F*) and lineation (*L*) values (Figure 4f) is also indicative of oblate magnetic fabric except for site FT32. It is worth to note that the *F* values in synorogenic deposits are the highest measured in the studied area, distinctly higher than those recorded in preorogenic and postorogenic deposits.

In order to test if the directions of K_{max} and K_{int} can be statically distinguished even in undisturbed sediments with strongly oblate AMS ellipsoids, we performed a bootstrap statistics analysis of eigenvalue and eigenvector

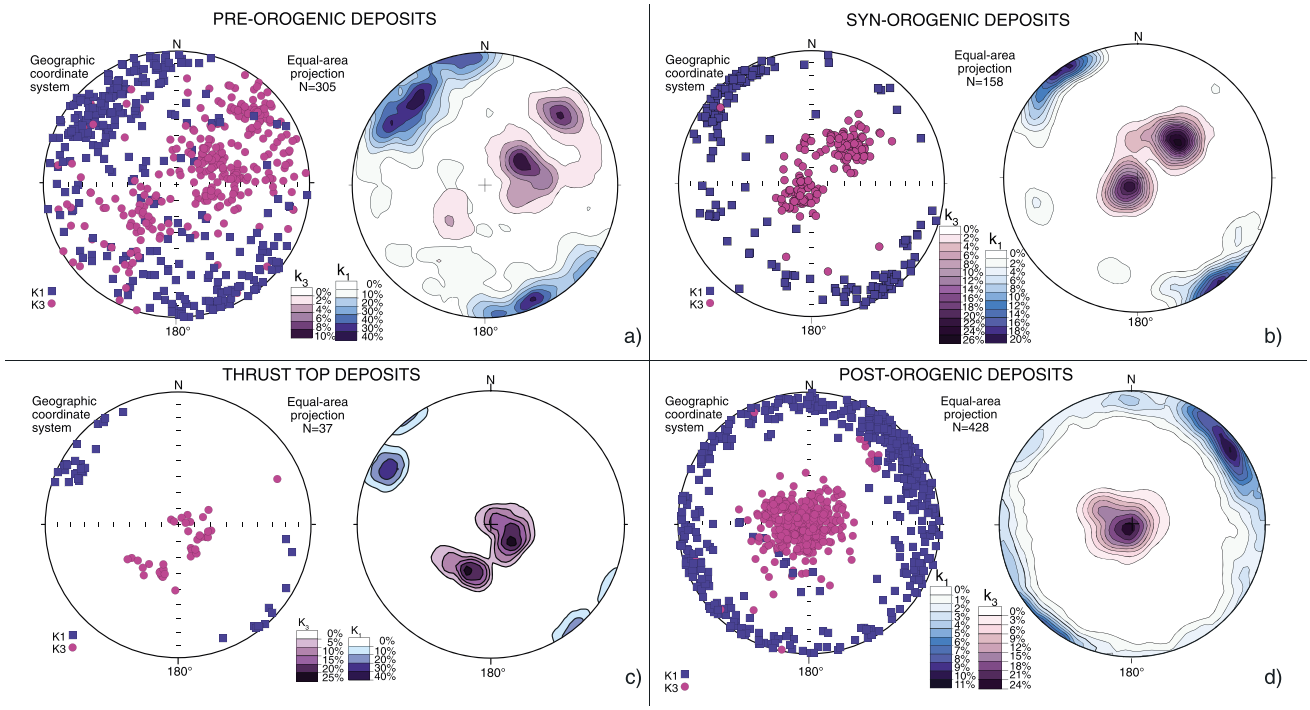

Figure 6. AMS results from all investigated sites plotted on equal area projections in geographic coordinates. The distribution of the K_{max} and K_{min} parameters is shown for preorogenic, synorogenic, thrust top, and postorogenic deposits. Blue squares indicate K_{max}, and purple circles indicate K_{min}. Contours of variable color represent the distribution of percentage densities of these two axes. The postorogenic deposits include data from Cava Serredi in *Sarti et al.* [1995].

distributions [*Constable and Tauxe*, 1990] (software aniso_magic.py in QuickMagic by *Tauxe* [2015]). The results, plotted in Figure 5, show that K_{max} and K_{int} distributions are statistically distinct for all four sedimentary units. In detail, the postorogenic deposits are characterized by oblate fabric, while preorogenic, synorogenic, and thrust top deposits show a triaxal fabric. The postorogenic deposits show a highly oblate AMS ellipsoid, with a vertical K_{min}.

4.3. AMS Directions

The overall set of data shows a distinct distribution of magnetic foliation and magnetic lineation in the different tectonic settings (Figure 6). In particular, in preorogenic, synorogenic, and thrust top deposits magnetic foliation forms a well-shaped girdle distribution oriented NE-SW and a well-grouped magnetic lineation oriented NW-SE (Figures 6a–6c). On the other hand, in postorogenic deposits the magnetic foliation is only slightly deviated from a subhorizontal distribution along the NE-SW direction and the magnetic lineation is more dispersed around a NE-SW direction (Figure 6d). This distinct orientation of magnetic lineation and foliation in postorogenic and in preorogenic, synorogenic, and thrust top deposits clearly suggests that the orientation of AMS principal axes is mostly related to the different tectonic processes that affected the Apennine chain and the Tyrrhenian margin during the Neogene. At the site level, the directions of the principal axes of the AMS ellipsoids are often tightly grouped with a well-defined magnetic foliation plane and magnetic lineation as shown in Figure 7. The magnetic foliation is generally parallel to the bedding plane except for a few samples from the preorogenic pelagic carbonates where the magnetic foliation is orthogonal to the bedding plane. In these cases, this orientation is most probably related to the presence of cleavage planes not visible at the outcrop scale or to the crystal growth of diagenetic hematite with the crystallographic basal plane perpendicular to bedding [*Lowrie and Hirt*, 1987]. Moreover, most of the sites clearly show distinct magnetic lineation as defined by the clustering of the K_{max} (Figure 7). In particular, in the following discussion, the orientation of the magnetic lineation is considered as reasonably well defined for samples in which the semiangle of the 95% confidence ellipse in the K_{max}-K_{int} plane (E_{1-2}) does not exceed 26.5° (Table 1) [*Jelinek*, 1977].

Accordingly, the lineation is well defined for 12 sites (out of 19 sites) of the preorogenic deposits, for 9 sites (out of 12) of the synorogenic deposits, for all the 3 sites sampled in thrust top deposits, and for 15

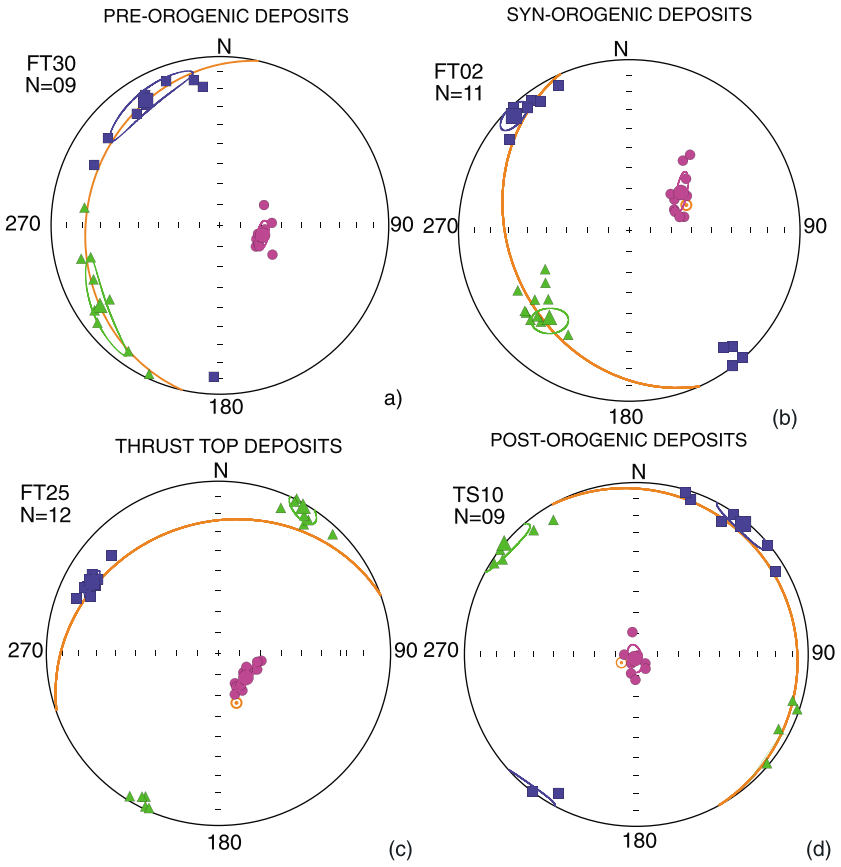

Figure 7. Magnetic anisotropy data from four representative sites (equal area Schmidt projection, lower hemisphere). The squares, triangle, and dots represent K_{max}, K_{int}, and K_{min}, respectively. The ellipses indicate the 95% region around the principal susceptibility axes. The orange line indicates the bedding plane. Orange circle with dot indicates the pole to bedding.

postorogenic sites (out of 29). All sites with poorly defined magnetic lineation have been discarded from further analyses. The orientation of the magnetic lineation is significantly different in preorogenic, synorogenic, thrust top deposits, and in the postorogenic sediments of extensional basins (Figure 6). Furthermore, in preorogenic and synorogenic units (Figures 7a and 7b) and in the thrust top deposits (Figure 7c) the magnetic lineation clusters subparallel to the strike of the magnetic foliation, oriented NNW-SSE to NW-SE. Conversely, the postorogenic sediments show a cluster of magnetic lineation around the NE-SW direction (Figure 7d).

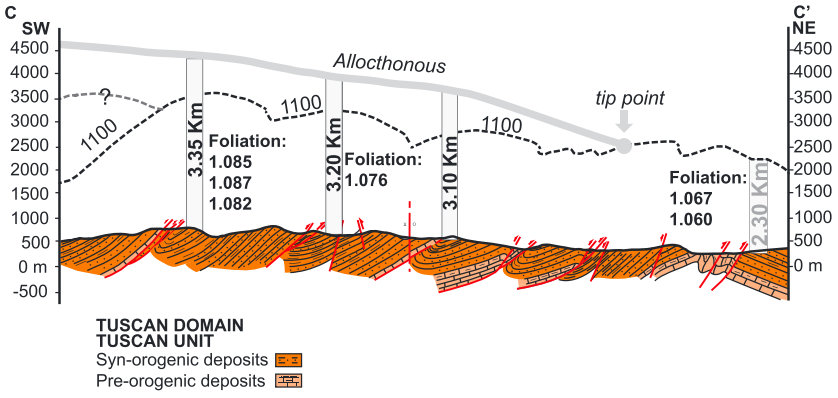

Figure 8. Geological cross section *C-C'* (trace in Figure 1) [after *Caricchi et al.,* 2015] showing the distributions of tectonic load and magnetic foliation values. Note the decreasing foliation values in correspondence of decreasing tectonic load.

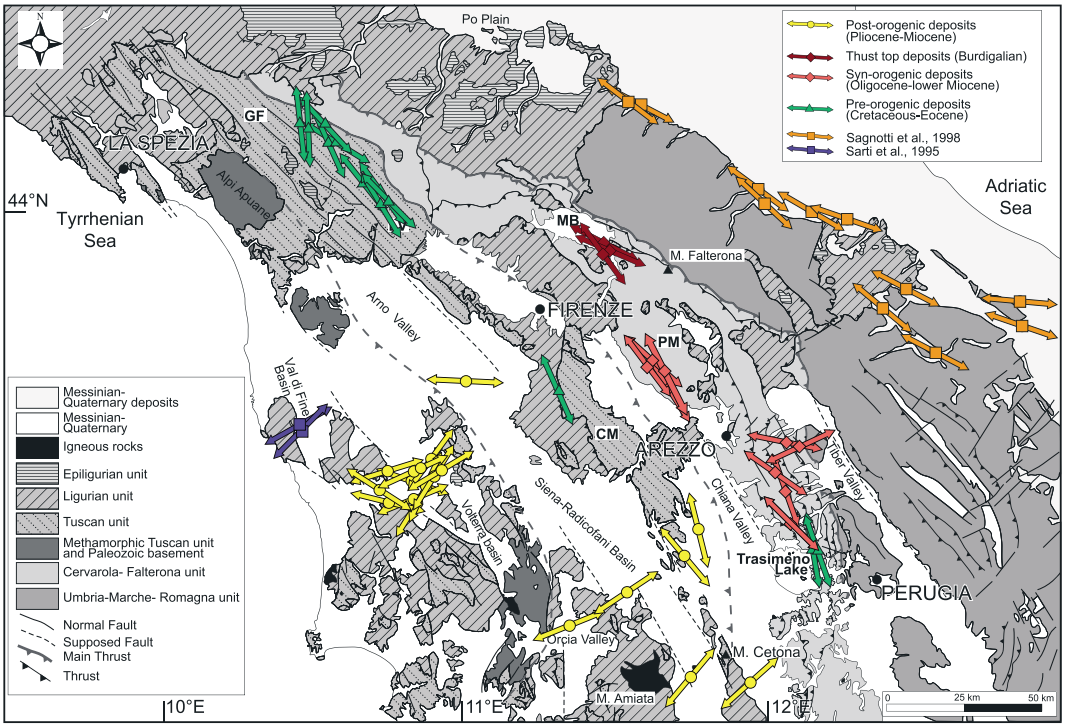

Figure 9. Orientation of the computed magnetic lineation for sites where $E_{1-2} < 26.5°$ (see text). Note the variation between the Tuscan Tyrrhenian margin and internal arc of Northern Apennines.

5. Discussion

5.1. The Magnetic Foliation

All the sites show a well-defined magnetic foliation parallel to the bedding plane. This magnetic foliation is related to sedimentary and compaction processes and appears to be strongly dependent on the lithology of the samples and on the sedimentary and tectonic loading acting at the sampling site. The lithological control is well evident in the different degrees of oblateness (represented by *T* and *F* parameters), with less oblate ellipsoids detected in the preorogenic and thrust top sediments of the Apennine units and more oblate in the synorogenic units of the Apennine foredeep basins. This difference clearly reflects the different carbonate and phyllosilicate contents observed in the different units. The high *T* and *F* values observed in the synorogenic units are clearly related to the large paramagnetic (phyllosilicates) content, whereas the low oblateness observed in preorogenic and thrust top units is mostly due to the large carbonate content in these rocks. We also suggest that the flattening degree is related to the sedimentary/tectonic load, which enhances the preferred orientation of phyllosilicates within the bedding planes. In order to test this hypothesis, magnetic foliation values obtained for clayey synorogenic sediments from the different thrust sheets are reported in a geological cross section of the Tuscan foredeep basin where the sedimentary/tectonic load was previously estimated (Figure 8) [*Caricchi et al.*, 2015]. Magnetic foliation values decrease moving from SW toward NE along the cross section, in correspondence with a reduction of tectonic load as estimated on the basis of geological and thermal maturity data [*Caricchi et al.*, 2015]. This suggests that besides a lithological control due to the carbonate content, the *F* parameter is directly related to the compaction process, as a consequence of the sedimentary/tectonic burial depths reached by the sediments. This inference is also supported by the low *F* values measured in clayey postorogenic deposits, which never experienced significant tectonic loads. Conversely, the low *F* values measured in preorogenic and thrust top deposits, which underwent a significant tectonic load but have high carbonate content in the rock matrix, indicate that caution is necessary in the tectonic interpretation of the AMS data in different lithologies since variable proportions of the diamagnetic and paramagnetic fractions may affect the magnetic fabric development.

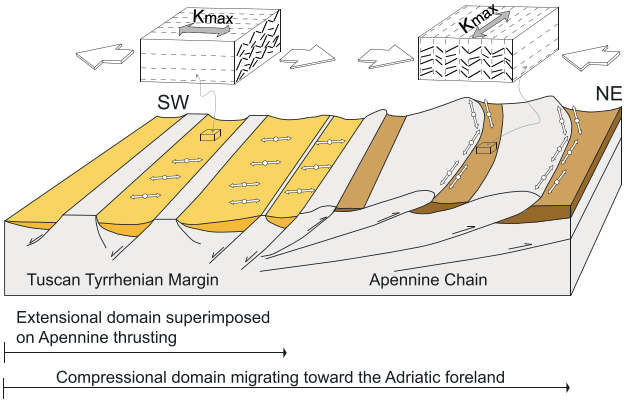

Figure 10. Schematic cross section with magnetic lineation direction across the Northern Apennines.

5.2. The Magnetic Lineation

The well-defined magnetic lineations ($E_{1-2} < 26.5°$) are reported in Figure 9 together with the results previously reported by *Sagnotti et al.* [1998] and *Sarti et al.* [1995]. Two different patterns are observed. In the units involved in the Apennine deformation (preorogenic, synorogenic, and thrust top units of the Apennine chain), the orientation of the magnetic lineation follows the curved shape of the Northern Apennines from N-S in the southern sector to NW-SE in the northern sector of the chain, being systematically parallel to the orientation of the main tectonic structures of the arc. This parallelism is observed both in the internal (Tuscan and Cervarola-Falterona units) and in the external (Umbria-Marche-Romagna unit) portions of the arc, which are characterized by different amount and age of deformation. Only two sites (FT09 and FT10) present an anomalous orientation with respect to the main trend with the lineation perpendicular to the regional trend fold axes, possibly indicating that these sites are affected by local extensional faults.

In the postorogenic units of the Tuscan Tyrrhenian margin, the magnetic lineations are mostly oriented NE-SW to E-W, almost orthogonal to the main basin-bounding extensional faults of the area. This geometry has been observed both in the more internal extensional basins (Val di Fine Volterra [*Sarti et al.*, 1995]), which rifted during the late Miocene, and in the more external basins (Orcia and Siena-Radicofani), which rifted mainly during the Pliocene. Only in a few sites, the magnetic lineation is oriented NW-SE, almost parallel to the main trend of the Tyrrhenian margin extensional basins. This anomalous orientation can be due to the presence of NE-SW normal faults, which represent the main elements of extensional transfer basins NE-SW oriented [*Sagnotti et al.*, 1994; *Faccenna et al.*, 1994] or can be due to the complex geometry of low-angle normal faults recognized in the area [*Maffione et al.*, 2012].

5.3. The Magnetic Fabric in the Apennine Thrust Belt and in the Extensional Tyrrhenian Margin

Figure 9 shows that the relationship between the magnetic fabric and the main tectonic structures is clearly distinctive in the sites within the compressional regime of the Northern Apennine fold-and-thrust belt compared to the extensional regime in basins associated with the Tuscan Tyrrhenian margin.

In the preorogenic, synorogenic, and thrust top deposits, K_{min} is distributed along a NE-SW oriented girdle, with a progressive decrease in the amount of girdling from the preorogenic to synorogenic and thrust top deposits (Figures 6a–6c). This pattern reflects the variable structural complexity and degree of deformation of the three different tectonostratigraphic deposits. In these three domains, K_{max} is oriented along the strike of the magnetic foliation and parallel to the regional fold axis described by the NE-SW girdling of the magnetic foliation (Figurea 6a–6c). Conversely, in the postorogenic deposits K_{min} is subvertical (except in TS18), with a slight girdling along a NE-SW direction. K_{max} also shows a prevalent distribution along the NE-SW axis in the foliation plane (Figure 6d). In postorogenic deposits the magnetic lineation mostly lies on the dip of the bedding plane, which is parallel to the magnetic foliation plane (Figure 6d).

This peculiar geometry indicates (i) a distinctive geometrical relationship between the orientation of magnetic lineation and magnetic foliation in compressional and extensional tectonic settings and (ii) a different relationship between the orientation of the magnetic lineation and the main tectonic structures in fold-and-thrust belts (where magnetic lineation parallels the main tectonic elements) and in extensional basins (where the magnetic lineation is orthogonal to the main tectonic elements) [*Mattei et al.*, 1997].

5.4. The Origin of Magnetic Lineation and the Tectonic Evolution of the Northern Apennines

In the Northern Apennines a direct relationship between the orientation of magnetic lineation and the main tectonic structures is observed in both extensional and compressional tectonic settings (Figure 10). This relationship exists in sedimentary units that differ in age, lithology, magnetic mineralogy, and sedimentary environment suggesting that the observed magnetic lineations result from tectonic deformation rather than from depositional processes. The origin of magnetic lineation in poorly deformed sediments from fold-and-thrust belts has been discussed in a large number of papers and has been generally considered as an intersection lineation between the bedding plane and an incipient cleavage developed during the early stages of LPS (see *Pares* [2015] for a recent review). On the other side, other studies carried out in "undeformed" sediments from extensional basins suggest that the magnetic lineation develops at the early stages of deformation and is related to reorientation of the basal planes of the phyllosilicate grains in response to the progressive extension. In this case the magnetic lineation is an intersection lineation resulting from the girdling of the phyllosilicates basal planes with the common axis of their intersection parallel to the stretching direction [*Cifelli et al*., 2004, 2005]. On this basis we propose that in the Northern Apennine the magnetic lineation initially formed during the early phases of LPS as described above. Subsequently, during Oligocene-lower Miocene time the Tuscan units were incorporated in the orogenic wedge, which progressively involved the more external sector of the chain. During this process, the magnetic lineation passively rotated counterclockwise to follow the formation of the Northern Apennine arc [*Caricchi et al*., 2014]. The parallelism with the main tectonic structures of the chain was therefore maintained. This process accompanied the progressive foreland migration of the Northern Apennine thrust front, giving rise to the formation of a tectonic magnetic lineation in the more external Umbria-Marche-Romagna units [*Sagnotti et al*., 1998]. The latter also underwent subsequent rotations around the vertical axis, which passively rotated the magnetic lineation together with the compressional structures after late Miocene times [*Speranza et al*., 1997].

The progressive foreland migration of the Northern Apennine chain was accompanied at the rear of the chain by the opening of extensional sedimentary basins, which formed progressively from the Tuscan Tyrrhenian margin (late Miocene) to the Umbria-Marche-Romagna sector (late Pliocene-lower Pleistocene) of the Apennine chain. These areas were progressively affected by NW-SE oriented normal faulting, which dissected the Apennine units and formed extensional, fault-bounded, sedimentary basins infilled by postorogenic sedimentary sequences. During this process a magnetic lineation oriented orthogonal to the normal fault direction was acquired in the different extensional basins of the Tuscan Tyrrhenian margin, which were not affected by any significant rotation around vertical axis [*Lowrie and Alvarez*, 1979; *Hirt and Lowrie*, 1988; *Sagnotti et al*., 1994; *Sarti et al*., 1995; *Mattei et al*., 1996]. It is worth to note that in the Apennine units the magnetic fabric acquired during the compressional deformation was not modified by the subsequent extensional tectonics, further demonstrating that in the Apennine chain the observed magnetic fabric formed during the early stages of deformation.

6. Conclusions

In this study, we report on new AMS data from different sedimentary units collected in the same orogenic system. The origin of magnetic fabric may be defined considering the AMS results in the various tectonic settings. In particular, the analyzed sediment showed a predominant magnetic foliation parallel to the bedding plane, indicating that the magnetic fabric is mainly due to the compaction process during diagenesis and it is also directly proportional to the amount of tectonic load experienced by the sediments during the orogenesis. The magnetic lineation recorded in the sites of the internal arc of Northern Apennine chain is parallel to the trend of folds and thrust faults, suggesting that it has a tectonic origin and it was most likely acquired during the incipient phases of LPS. Conversely, in the Tuscan Tyrrhenian margin, the magnetic lineation is perpendicular to the main extensional faults and represents the stretching direction of the extensional deformation. This study reveals that the original sedimentary magnetic fabric was partly overprinted by a preferred reorientation of minerals in the rock matrix by an incipient deformation related to compressional and extensional phases in the same orogeny, the Northern Apennines. In a more general sense, our results verify the distinctive relationships between the orientation of magnetic lineation and the main tectonic features in extensional and compressional tectonic regimes, highlighting the large potential of the AMS method for studying tectonic deformation in poorly deformed rocks at both the local and regional scales.

Acknowledgments
We are grateful to A. Winkler for useful discussions and help during the laboratory measurements. We would like to thank S. Corrado and L. Aldega for the constructive discussion on the relationship between magnetic fabric and tectonic load. L. Aldega is also acknowledged for the X-ray analyses. F. Speranza and F. Sani are kindly acknowledged for their precious help in the field. We thank A.M. Hirt and an anonymous reviewer for their constructive comments. This research has been funded by MIUR-PhD grant 2010–2012 to C. Caricchi and by Italian MIUR through Cofin_2010-2011 (project 2010TT22SC_003) grant to M. Mattei. The database containing all materials needed to produce the results is available from the authors upon request.

References

Alimohammadian, H., Z. Hamidi, A. Aslani, A. Shahidi, F. Cifelli, and M. Mattei (2013), A tectonic origin of magnetic fabric in the Shemshak Group from Alborz Mts. (northern Iran), *J. Asian Earth Sci.*, *73*, 419–428.

Aubourg, C., P. Rochette, and P. Vialon (1991), Subtle stretching lineation revealed by magnetic fabric of Callovian–Oxfordian black shales (French Alps), *Tectonophysics*, *185*, 211–223.

Averbuch, O., D. Frizon de Lamotte, and C. Kissel (1992), Magnetic fabric as a structural indicator of the deformation path within a fold-thrust structure: A test case from the Corbieres (NE Pyrenees, France), *J. Struct. Geol.*, *14*, 461–474.

Baas, J. H., E. A. Hailwood, W. D. McCaffrey, M. Kay, and R. Jones (2007), Directional petrological characterization of deep-marine sandstones using grain fabric and permeability anisotropy: Methodologies, theory, application and suggestions for integration, *Earth Sci. Rev.*, *82*, 101–142.

Baldacci, F., P. Elter, E. Giannini, G. Giglia, A. Lazzarotto, R. Nardi, and M. Tongiorgi (1967), Nuove osservazioni sul problema della Falda Toscana e sulla interpretazione dei flysch arenacei tipo "Macigno" dell'Appennino settentrionale, *Mem. Soc. Geol. Ital.*, *6*(2), 213–244.

Bally, A. W., L. Burbi, C. Cooper, and R. Ghelardoni (1986), Balanced sections and seismic reflection profiles across the Central Apennines, *Mem. Soc. Geol. Ital.*, *35*, 257–310.

Balsamo, F., F. Storti, B. Piovano, F. Salvini, F. Cifelli, and C. Lima (2008), Time dependent structural architecture of subsidiary fracturing and stress pattern in the tip region of an extensional growth fault system, Tarquinia basin, Italy, *Tectonophysics*, *454*, 54–69, doi:10.1016/j.tecto.2008.04.011.

Barchi, M. R., A. De Feyter, B. Magnani, G. Minelli, G. Pialli, and B. Sotera (1998a), The structural style of the Umbria-Marche fold and thrust belt, *Mem. Soc. Geol. Ital.*, *52*, 557–578.

Barchi, M. R., A. De Feyter, B. Magnani, G. Minelli, G. Pialli, and B. Sotera (1998b), Extensional tectonics in the Northern Apennines (Italy): Evidence from the CROP03 deep seismic reflection line, *Mem. Soc. Geol. Ital.*, *52*, 528–538.

Battaglia, S., L. Leoni, and F. Sartori (2002), Mineralogical and grain size composition of clays developing calanchi and biancane erosional landform, *Geomorfology*, *49*, 153–170.

Boccaletti, M., M. Coli, F. A. Decandia, E. Giannini, and A. Lazzarotto (1980), Evoluzione dell'Appennino Settentrionale secondo un nuovo modello strutturale, *Mem. Soc. Geol. Ital.*, *21*, 359–373.

Borradaile, G. J. (1988), Magnetic fabrics, petrofabrics and strain, *Tectonophysics*, *156*, 1–20.

Borradaile, G. J., and B. Henry (1997), Tectonic applications of magnetic susceptibility and its anisotropy, *Earth Sci. Rev.*, *42*, 49–93.

Bortolotti, V., G. Principi, and B. Treves (2001), Ophiolites, Ligurides and the tectonic evolution from spreading to convergence of Mesozoic western Tethys segment, in *Anatomy of an Orogen: The Appennines and Adjacent Mediterranean Basins*, edited by G. B. Vai and I. P. Martini, pp. 151–164, Kluwer Acad., London.

Cai, J., T. Xiaodong, and Y. Wu (2014), Magnetic fabric and paleomagnetism of the Middle Triassic siliciclastic rocks from the Nanpanjiang Basin, South China: Implications for sediment provenance and tectonic process, *J. Asian Earth Sci.*, *80*, 134–147.

Caricchi, C., F. Cifelli, L. Sagnotti, F. Sani, F. Speranza, and M. Mattei (2014), Paleomagnetic evidence for a post-Eocene 90° CCW rotation of internal Apennine units: A linkage with Corsica-Sardinia rotation?, *Tectonics*, *33*, 374–392, doi:10.1002/2013TC003364.

Caricchi, C., L. Aldega, and S. Corrado (2015), Reconstruction of maximum burial along the Northern Apennines thrust wedge (Italy) by indicators of thermal exposure and modeling, *Geol. Soc. Am. Bull.*, *127*, 428–442, doi:10.1130/B30947.1.

Cerrina Feroni, A., G. Ottria, P. Martinelli, and L. Martelli (2002), *Structural Geological Map of the Emilia-Romagna Apennines, 1:250,000 Scale*, S.EL.CA, Firenze.

Channell, J. E. T., B. D'Argenio, and F. Horvath (1979), Adria, the African promontory, in Mesozoic Mediterranean palaeogeography, *Earth Sci. Rev.*, *15*, 213–292.

Chiaraluce, L., et al. (2004), Complex normal faulting in the Apennines thrust-and-fold belt: The 1997 seismic sequence in central Italy, *Bull. Seismol. Soc. Am.*, *94*, 99–116.

Cifelli, F., F. Rossetti, M. Mattei, A. M. Hirt, R. Funiciello, and L. Tortorici (2004), An AMS, structural and paleomagnetic study of quaternary deformation in eastern Sicily, *J. Struct. Geol.*, *26*(1), 29–46, doi:10.1016/S0191-8141(03)00092-0.

Cifelli, F., M. Mattei, M. Chadima, A. M. Hirt, and A. Hansen (2005), The origin of tectonic lineation in extensional basins: Combined neutron texture and magnetic analyses on "undeformed" clays, *Earth Planet. Sci. Lett.*, *235*, 62–78.

Cifelli, F., F. Rossetti, and M. Mattei (2007), The architecture of brittle postorogenic extension: Results from an integrated structural and paleomagnetic study in north Calabria (southern Italy), *Geol. Soc. Am. Bull.*, *119*, 221–239.

Cifelli, F., M. Mattei, M. Chadima, S. Lenser, and A. M. Hirt (2009), The magnetic fabric in "undeformed clays": AMS and neutron texture analyses from the Rif Chain (Morocco), *Tectonophysics*, *466*, 79–88, doi:10.1016/j.tecto.2008.08.008.

Cifelli, F., M. Mattei, H. Rashid, and J. Ghalamghash (2013), Right-lateral transpressional tectonics along the boundary between Lut and Tabas blocks (Central Iran), *Geophys. J. Int.*, *193*, 1153–1165, doi:10.1093/gji/ggt070.

Cifelli, F., P. Ballato, H. Alimohammadian, J. Sabouri, and M. Mattei (2015), Tectonic magnetic lineation and oroclinal bending of the Alborz range: Implications on the Iran-Southern Caspian geodynamics, *Tectonics*, *34*, 116–132, doi:10.1002/2014TC003626.

Collettini, C., N. De Paola, H. R. Holdsworth, and M. R. Barchi (2006), The development and behaviour of low-angle normal faults during Cenozoic asymmetric extension in the Northern Apennines, Italy, *J. Struct. Geol.*, *28*, 333–352.

Constable, C., and L. Tauxe (1990), The bootstrap for magnetic susceptibility tensors, *J. Geophys. Res.*, *95*(B6), 8383–8395, doi:10.1029/JB095iB06p08383.

Costa, E., G. Pialli, and G. Plesi (1998), Foreland basins of the Northern Apennines: Relationships with passive subduction of the Adriatic lithosphere, *Mem. Soc. Geol. Ital.*, *52*, 595–606.

Dall'Olio, E., F. Felletti, and G. Muttoni (2013), Magnetic fabric analysis as a tool to constrain mechanisms of deep-water mudstone deposition in the Marnoso Arenacea Formation (Miocene, Italy), *J. Sediment. Res.*, *83*, 170–182.

Day, R., M. Fuller, and V. A. Schmidt (1977), Hysteresis properties of titanomagnetite: Grain size and compositional dependence, *Phys. Earth Planet. Inter.*, *13*, 260–267.

Debacker, T. N., P. Robion, and M. Sintubin (2004), The anisotropy of magnetic susceptibility (AMS) in low-grade, cleaved pelitic rocks: Influence of cleavage/bedding angle and type and relative orientation of magnetic carriers, in *Magnetic Fabrics: Methods and Applications*, edited by F. Martin-Hernandez et al., *Geol. Soc., London Spec. Publ.*, 238, 77–107.

Debacker, T. N., A. M. Hirt, M. Sintubin, and P. Robion (2009), Differences between magnetic and mineral fabrics in low-grade, cleaved siliciclastic pelites: A case study from the Anglo-Brabant Deformation Belt (Belgium), *Tectonophysics*, *466*, 32–46.

Dewey, J. F., M. L. Helman, E. Turco, D. H. W. Hutton, and S. D. Knott (1989), Kinematics of the western Mediterranean, in *Alpine Tectonics*, edited by M. P. Coward, D. Dietrich, and R. G. Park, *Geol. Soc, London Spec. Publ.*, 45, 265–283.

Dunlop, D. J. (2002), Theory and application of the Day plot (Mrs/Ms versus Hcr/Hc): 1. Theoretical curves and tests using titanomagnetite data, *J. Geophys. Res.*, *107*(B3), 2056, doi:10.1029/2001JB000486.
Ellwood, B. B. (1980), Application of the anisotropy of magnetic susceptibility method as an indicator of bottom water flow direction, *Mar. Geol.*, *34*, 83–90.
Elter, P. (1975), L'ensemble ligure, *Bull. Soc. Geol. Fr.*, *17*, 984–997.
Faccenna, C., A. Bruni, R. Funiciello, M. Mattei, and L. Sagnotti (1994), Evolution of a transfer-related basin: The Ardea basin (Latium, central Italy), *Basin Res.*, *6*, 35–46, doi:10.1111/j.1365-2117.1994.tb00073.x.
Faccenna, C., C. Piromallo, A. Crespo-Blanc, L. Jolivet, and F. Rossetti (2004), Lateral slab deformation and the origin of the western Mediterranean arcs, *Tectonics*, *23*, TC1012, doi:10.1029/2002TC001488.
Festa, A., G. A. Pini, Y. Dilek, G. Codegone, L. Vezzani, F. Ghisetti, C. Lucente, and K. Ogata (2010), Peri-Adriatic melanges and their evolution in the Tethyan realm, *Int. Geol. Rev.*, *52*, 369–403.
Graham, J. W. (1966), Significance of magnetic anisotropy in Appalachian sedimentary rocks, in *The Earth Beneath the Continents*, *Geophys. Monogr.*, vol. 10, edited by J. S. Steinhart and T. J. Smith, pp. 627–648, AGU, Washington, D. C.
Hamilton, N., and A. I. Rees (1970), The use of magnetic fabric in palaeocurrent estimation, in *Palaeogeophysics*, edited by S. K. Runcorn, pp. 445–464, Academic Press, London.
Hirt, A. M., and W. Lowrie (1988), Paleomagnetism of the Umbrian-Marches orogenic belt, *Tectonophysics*, *146*, 91–103.
Hirt, A. M., K. E. Evans, and T. Engeldr (1995), Correlation between magnetic anisotropy and fabric for Devonian shales on the Appalachian Plateau, *Tectonophysics*, *247*, 121–132.
Hirt, A., M. Julivert, and J. Soldevila (2000), Magnetic fabric and deformation in the Navia–Alto Sil slate belt, northwestern Spain, *Tectonophysics*, *320*, 1–16.
Housen, B. A., and B. A. Van der Pluijm (1991), Slaty cleavage development and magnetic anisotropy fabrics (AMS and ARMA), *J. Geophys. Res.*, *96*(B6), 9937–9946, doi:10.1029/91JB00605.
Housen, B. A., C. Richter, and B. A. Van der Pluijm (1993), Composite magnetic anisotropy fabrics: Experiments, numerical models, and implications for the quantification of rock fabrics, *Tectonophysics*, *220*, 1–12.
Hrouda, F. (1982), Magnetic anisotropy of rocks and its application in geology and geophysics, *Geophys. Surv.*, *5*, 37–82.
Hrouda, F., and S. Kahan (1991), The magnetic fabric relationship between sedimentary and basement nappes in the High Tatra Mountains, N Slkovakia, *J. Struct. Geol.*, *13*, 432–442.
Jelinek, V. (1981), Characterization of the magnetic fabrics of rocks, *Tectonophysics*, *79*, 63–67.
Jelínek, V., and V. Kropáček (1978), Statistical processing of anisotropy of magnetic susceptibility measured on groups of specimens, *Stud. Geophys. Geod.*, *22*, 50–62.
Jolivet, L., et al. (1998), Midcrustal shear zones in postorogenic extension: Example from the northern Tyrrhenian Sea, *J. Geophys. Res.*, *103*(B6), 12,123–12,160, doi:10.1029/97JB03616.
Kanamatsu, T., E. Herrero-Bervera, and A. Taira (2001), Magnetic fabrics of soft-sediment folded strata within a Neogene accretionary complex, the Miura group, central Japan, *Earth Planet. Sci. Lett.*, *187*, 333–343.
Kissel, C., E. Barrier, C. Laj, and T. Q. Lee (1986), Magnetic fabric in "undeformed" marine clays from compressional zones, *Tectonics*, *5*(5), 769–781, doi:10.1029/TC005i005p00769.
Kissel, C., C. Laj, B. Lehman, L. Labyrie, and V. Bout-Roumazeilles (1997), Changes in the strength of the Iceland–Scotland Overflow Water in the last 200,000 years: Evidence from magnetic anisotropy analysis of core SU90-33, *Earth Planet. Sci. Lett.*, *152*, 25–36.
Kissel, C., C. Laj, M. Kienast, T. Bolliet, A. Holbourn, P. Hill, W. Kuhnt, and P. Braconnot (2010), Monsoon variability and deep oceanic circulation in the western equatorial Pacific over the last climatic cycle: Insights from sedimentary magnetic properties and sortable silt, *Paleoceanography*, *25*, PA3215, doi:10.1029/2010PA001980.
Kligfield, R., W. H. Owens, and W. Lowrie (1981), Magnetic susceptibility anisotropy, strain, and progressive deformation in Permian sediments from the Maritime Alps (France), *Earth Planet. Sci. Lett.*, *55*, 181–189.
Larrasoaña, J. C., E. L. Pueyo, and J. M. Parés (2004), An integrated AMS, structural palaeo- and rock-magnetic study of Eocene marine marls from the Jaca-Pamplona basin (Pyrenees, N Spain): New insights into the timing of magnetic fabric acquisition in weakly deformed mudrocks, in *Magnetic Fabric: Methods and Applications*, edited by F. Martín-Hernández et al., *Geol. Soc., London Spec. Publ.*, 238, 127–143.
Larrasoaña, J. C., M. Gomez-Paccard, S. Giralt, and A. P. Roberts (2011), Rapid locking of tectonic magnetic fabrics in weakly deformed mudrocks, *Tectonophysics*, *507*, 16–25.
Lee, T., C. Kissel, C. Laj, C. S. Horng, and Y. T. Lue (1990), Magnetic fabric analysis of the Plio-Pleistocene sedimentary formations of the Coastal Range of Taiwan, *Earth Planet. Sci. Lett.*, *98*, 23–32.
Lowrie, W. (1990), Identification of ferromagnetic minerals in a rock by coercivity and unblocking temperature properties, *Geophys. Res. Lett.*, *17*(2), 159–162, doi:10.1029/GL017i002p00159.
Lowrie, W., and A. M. Hirt (1987), Anisotropy of magnetic susceptibility in the Scaglia Rossa pelagic limestone, *Earth Planet. Sci. Lett.*, *82*, 349–356.
Lowrie, W., and W. Alvarez (1979), Paleomagnetism and rock magnetism of the Pliocene rhyolite at San Vincenzo, Tuscany, Italy, *J. Geophys.*, *45*, 417–432.
Lunemburg, C. M., S. A. Lampert, H. D. Lebit, A. M. Hirt, M. Casey, and W. Lowrie (1999), Magnetic anisotropy, rock fabrics and finite strain in deformed sediments of SW Sardinia (Italy), *Tectonophysics*, *307*, 51–74.
Maffione, M., S. Pucci, L. Sagnotti, and F. Speranza (2012), Magnetic fabric of Pleistocene continental clays from the hanging-wall of an active low-angle normal fault (Altotiberina Fault, Italy), *Int. J. Earth Sci. (Geol. Rundschau)*, *101*, 849–861, doi:10.1007/s00531-011-0704-9.
Malinverno, A., and W. B. F. Ryan (1986), Extension in the Tyrrhenian Sea and shortening in the Apennines as result of arc migration driven by sinking of the lithosphere, *Tectonics*, *5*(2), 227–245, doi:10.1029/TC005i002p00227.
Marroni, M., G. Molli, G. Ottria, and L. Pandolfi (2001), Tectono- sedimentary evolution of the External Liguride units (Northern Apennines, Italy): Insights in the pre-collisional history of a fossil ocean-continent transition zone, *Geod. Acta*, *14*(5), 307–320, doi:10.1016/S0985-3111(00)01050-0.
Mattei, M., C. Kissel, and R. Funiciello (1996), No tectonic rotation of the Tuscan Tyrrhenian margin (Italy) since Late Messinian, *J. Geophys. Res.*, *101*(B2), 2835–2845, doi:10.1029/95JB02398.
Mattei, M., L. Sagnotti, C. Faccenna, and R. Funiciello (1997), Magnetic fabric of weakly deformed clayey sediments in the Italian peninsula: Relationships with compressional and extensional tectonics, *Tectonophysics*, *271*, 107–122.
Mattei, M., N. D'Agostino, I. Zananiri, D. Kondopoulou, S. Pavlides, and V. Spatharas (2004), Tectonic evolution of fault-bounded continental blocks: Comparison of paleomagnetic and GPS data in the Corinth and Megara basins (Greece), *J. Geophys. Res.*, *109*, B02106, doi:10.1029/2002TC001434.

Meneghini, F., F. Botti, L. Aldega, C. Boschi, S. Corrado, M. Marroni, and L. Pandolfi (2012), Hot fluid pumping along shallow-level collisional thrusts: The Monte Rentella Shear Zone, Umbria Apennine, Italy, *J. Struct. Geol.*, *37*, 36–52, doi:10.1016/j.jsg.2012.02.004.

Molli, G., G. Giorgetti, and M. Meccheri (2002), Tectono-metamorphic evolution of the Alpi Apuane Metamorphic Complex: New data and constraints for geodynamic models, *Boll. Soc. Geol. Ital.*, *1*, 789–800.

Oliva-Urcia, B., J. C. Larrasoaña, E. L. Pueyo, A. Gil, P. Mata, J. M. Parés, A. M. Schleicher, and Ó. Pueyo (2009), Disentangling magnetic subfabrics and their link to deformation processes in cleaved sedimentary rocks from the Internal Sierras (west central Pyrenees, Spain), *J. Struct. Geol.*, *31*(2), 163–176.

Oliva-Urcia, B., A. M. Casas, R. Soto, J. J. Villalaín, and K. Kodama (2010a), A transtensional basin model for the Organyà basin (central southern Pyrenees) based on magnetic fabric and brittle structures, *Geophys. J. Int.*, *184*(1), 111–130.

Oliva-Urcia, B., T. Román-Berdiel, A. M. Casas, E. L. Pueyo, and C. Osácar (2010b), Tertiary compressional overprint on Aptian-Albian extensional magnetic fabrics, North Pyrenean Zone, *J. Struct. Geol.*, *32*, 362–376.

Parés, J. M. (2004), How deformed are weakly deformed mudrocks? Insights from magnetic anisotropy. Magnetic fabric: Methods and applications, *Geol. Soc. London Spec. Publ.*, *238*, 191–205.

Parés, J. M. (2015), Sixty years of anisotropy of magnetic susceptibility in deformed sedimentary rocks, *Front. Earth Sci.*, *3*, 4, doi:10.3389/feart.2015.00004.

Parés, J. M., and B. A. Van der Pluijm (2002), Evaluating magnetic lineations (AMS) in deformed rocks, *Tectonophysics*, *350*, 283–298.

Parés, J. M., B. A. Van der Pluijm, and J. Dinares-Turell (1999), Evolution of magnetic fabrics during incipient deformation of mudrocks (Pyrenees, northern Spain), *Tectonophysics*, *307*, 1–14.

Parés, J. M., N. J. C. Hassold, D. K. Rea, and B. A. Van der Pluijm (2007), Paleocurrent directions from paleomagnetic reorientation of magnetic fabrics in deep-sea sediments at the Antarctic Peninsula Pacific margin (ODP Sites 1095, 1101), *Mar. Geol.*, *242*, 261–269.

Porreca, M., and M. Mattei (2012), AMS fabric and tectonic evolution of Quaternary intramontane extensional basins in the Picentini Mountains (Southern Apennines, Italy), *Int. J. Earth Sci.*, *101*, 787–802, doi:10.1007/s00531-011-0670-2.

Principi, G., and B. Treves (1984), Il sistema Corso-Appenninico come prisma di accezione. Riflessi sul problema generale del limite Alpi–Appennini, *Mem. Soc. Geol. Ital.*, *28*, 549–576.

Rees, A. I. (1965), The use of anisotropy of magnetic susceptibility in the estimation of sedimentary fabric, *Sedimentology*, *4*, 257–271.

Rees, A. I., and W. A. Woodall (1975), The magnetic fabric of some laboratory-deposited sediments, *Earth Planet. Sci. Lett.*, *25*, 121–130.

Rochette, P., M. J. Jackson, and C. Aubourg (1992), Rock magnetism and the interpretation of anisotropy of magnetic susceptibility, *Rev. Geophys.*, *30*(3), 209–226, doi:10.1029/92RG00733.

Sagnotti, L., and F. Speranza (1993), Magnetic fabric analysis of the Plio-Pleistocene clay units of Sant'Arcangelo basin, southern Italy, *Phys. Earth Planet. Inter.*, *77*, 165–176.

Sagnotti, L., C. Faccenna, R. Funiciello, and M. Mattei (1994), Magnetic fabric and structural setting of Plio-Pleistocene clayey units in an extensional regime: The Tyrrhenian margin of central Italy, *J. Struct. Geol.*, *16*, 1243–1257.

Sagnotti, L., F. Speranza, A. Winkler, M. Mattei, and R. Funiciello (1998), Magnetic fabric of clay sediments from the external northern Apennines (Italy), *Phys. Earth Planet. Inter.*, *105*, 73–93.

Sarti, G., F. Florindo, and L. Sagnotti (1995), Risultati di una indagine interdisciplinare (analisi di facies, biostratigrafia, magnetostratigrafia) svolta su due sezioni della Val di Fine (Toscana, Pisa) di età compresa tra il Miocene superiore ed il Pliocene inferiore, *Stud. Geol. Camerti*, *1995*(1), 593–600.

Schieber, J., and B. B. Ellwood (1988), Determination of basin wide paleocurrent patterns in a shale succession from anisotropy of magnetic susceptibility (AMS): A case study of the Mid-Proterozoic Newland Formation, Montana, *J. Sediment. Petrol.*, *58*, 830–835.

Soto, R., A. M. Casas-Sainz, J. J. Villalain, and B. Olivia-Urcia (2007), Mesozoic extension in the Basque-Cantabria basin (N Spain): Contribution from AMS and brittle mesostructure, *Tectonophysics*, *445*, 373–394.

Speranza, F., L. Sagnotti, and M. Mattei (1997), Tectonics of the Umbria-Marche-Romagna Arc (central northern Apennines, Italy): New paleomagnetic constraints, *J. Geophys. Res.*, *102*(B2), 3153–3166, doi:10.1029/96JB03116.

Taira, A. (1989), Magnetic fabric and depositional processes, in *Sedimentary Facies in the Active Plate Margins*, edited by A. Taira and F. Masuda, pp. 43–77, Terra Co., Tokyo.

Tang, Z., B. Huang, X. Dong, J. Ji, and Z. Ding (2012), Anisotropy of magnetic susceptibility of the Jingou River section: Implications for late Cenozoic uplift of the Tian Shan, *Geochem. Geophys. Geosyst.*, *13*, Q03022, doi:10.1029/2011GC003966.

Tarling, D. H., and F. Hrouda (1993), *The Magnetic Anisotropy of Rocks*, 217 pp., Chapman and Hall, London.

Tavani, S., and F. Cifelli (2010), Deformation pattern analysis and tectonic implications of a décollement level within the Central Apennines (Italy), *Geol. J.*, *45*, 582–596, doi:10.1002/gj.1198.

Veloso, E. E., R. Anma, O. Tsutomu, T. Komiya, S. Kagashima, and T. Yamazaki (2007), Paleocurrent patterns of the sedimentary sequence of the Taitao ophiolite constrained by anisotropy of magnetic susceptibility and paleomagnetic analyses, *Sediment. Geol.*, *201*, 446–460.

Weaver, R., A. P. Roberts, R. Flecker, and D. I. M. MacDonald (2004), Tertiary geodynamics of Sakhalin (NW Pacific) from anisotropy of magnetic susceptibility fabrics and paleomagnetic data, *Tectonophysics*, *379*, 25–42.

Weil, A. B., and A. Yonkee (2009), Anisotropy of magnetic susceptibility in weakly deformed red beds from the Wyoming salient, Sevier thrust belt: Relations to layer-parallel shortening and orogenic curvature, *Lithosphere*, *1*, 235–256.